



HAL
open science

An EGF-responsive neural circuit couples insulin secretion with nutrition in *Drosophila*

Eleonora Meschi, Pierre Léopold, Rénald Delanoue

► **To cite this version:**

Eleonora Meschi, Pierre Léopold, Rénald Delanoue. An EGF-responsive neural circuit couples insulin secretion with nutrition in *Drosophila*. *Developmental Cell*, 2019, 48 (1), pp.76-86.e5. 10.1016/j.devcel.2018.11.029 . hal-02313567

HAL Id: hal-02313567

<https://hal.sorbonne-universite.fr/hal-02313567>

Submitted on 11 Oct 2019

HAL is a multi-disciplinary open access archive for the deposit and dissemination of scientific research documents, whether they are published or not. The documents may come from teaching and research institutions in France or abroad, or from public or private research centers.

L'archive ouverte pluridisciplinaire **HAL**, est destinée au dépôt et à la diffusion de documents scientifiques de niveau recherche, publiés ou non, émanant des établissements d'enseignement et de recherche français ou étrangers, des laboratoires publics ou privés.

An EGF-responsive neural circuit couples insulin secretion with nutrition in *Drosophila*

Eleonora Meschi¹, Pierre Léopold^{1,2*} and Renald Delanoue¹

¹Université Côte d'Azur, CNRS, Inserm, Institute of Biology Valrose, Parc Valrose, 06108 Nice, France.

²present address: Institut Curie, PSL Research University, CNRS UMR3215, INSERM U934, UPMC Paris-Sorbonne, 26 Rue d'Ulm, 75005, Paris, France.

* corresponding author and lead contact: leopold@unice.fr

Running title: EGFR-driven neural circuitry controls insulin release in *Drosophila*

Summary (150 words max.)

Developing organisms use fine-tuning mechanisms to adjust body growth to ever-changing nutritional conditions. In *Drosophila*, the secretory activity of insulin-Producing Cells (IPCs) is central to couple systemic growth with amino acids availability. Here, we identify a subpopulation of inhibitory neurons contacting the IPCs (IPCs-connecting neurons, or ICNs) that play key role in this coupling. We show that ICNs respond to Growth Blocking Peptides (GBPs), a family of fat body-derived signals produced upon availability of dietary amino acids. We demonstrate that GBPs are atypical ligands for the fly EGF receptor (EGFR). Upon activation of EGFR by adipose GBPs, ICN-mediated inhibition of IPC function is relieved, allowing insulin secretion. Our study reveals an unexpected role for EGF-like metabolic hormones and EGFR signaling as critical modulators of neural activity, coupling insulin secretion to the nutritional status.

Key words

EGF, growth, insulin, inter-organ communication, nutrition, GBPs, neuronal circuit

Introduction

Developing organisms must evaluate their nutritional status, adapt growth and maintain energy homeostasis. In vertebrates, variations in the circulating levels of insulin and insulin-like growth factor 1 (IGF-I) trigger nutrient storage and release, and control systemic growth. Therefore, the release of insulin-like peptides by their producing cells is tightly regulated by nutrients. Alterations in this coupling is associated with major metabolic diseases and growth defect (Donadon et al., 2009).

Insulin-like peptides act on an evolutionary conserved pathway and serve the same physiological role in coupling nutrition and growth in all developing multicellular organisms. In *Drosophila*, eight Insulin-like peptides (Dilp1-8) have been identified. With the exception of Dilp8, which has distinct functions (Colombani et al., 2012), all the other Dilps carry out both the metabolic functions of the vertebrate insulin and the growth-promoting functions of IGFs, through a unique receptor (InR) and a conserved intracellular insulin/IGF signaling pathway (IIS) (Garofalo, 2002; Ikeya et al., 2002). In flies, the insulin-producing cells (IPCs), which are functionally related to the pancreatic beta cells, are found in the brain (Rulifson et al., 2002). The IPCs are peptidergic neurons, located in the median neurosecretory cluster (mNSC), producing at least four of the Dilps (Brogiolo et al., 2001; Ikeya et al., 2002; Liu et al., 2016). IPCs processes present at the surface of the heart tube release Insulin-like peptides into the hemolymph, inducing organ growth and controlling carbohydrate homeostasis (Rulifson et al., 2002).

During the growth period, IPC secretory activity is indirectly coupled to the nutrient status through an inter-organ communication involving the fat body (FB), a functional equivalent of vertebrate liver and white adipose tissue that acts as a nutrient sensor. This function relies on the amino acid sensor Target Of Rapamycin Complex 1 (TORC1) in the FB, controlling the production of fat body-derived signals (FBS) that remotely adjust Dilps secretion from the IPCs (Colombani et al., 2003; Géminard et al., 2009). Both growth-promoting and –inhibiting FBSs, produced in response to various nutritional cues, participate in this tight control. The cytokine Unpaired 2 (Upd2) and the small peptide CCHamide-2 (CCHa2) stimulate IPCs activity after sugar and/or lipid intakes (Rajan and Perrimon, 2012; Sano et al., 2015). In response to dietary amino acids, adipose cells release the Stunted (Sun)

peptide), which remotely activate brain Dilp secretion (Delanoue et al., 2016). The Growth Blocking Peptides 1 and 2 (GBP1, 2) were initially described as growth inhibitors, or activators depending on their concentration after injection in lepidopteran (Hayakawa, 1991; Hayakawa and Ohnishi, 1998). More recently, they were shown to work as *bona fide* growth factors produced by fat body cells in response to an amino acid signal and to stimulate Dilp secretion (Koyama and Mirth, 2016). Conversely, chronic exposure to a low protein diet induces the release of Tumor Necrosis Factor (TNF)- α from fat cells, which in turn represses brain *dilp2* expression (Agrawal et al., 2016).

These FBSs do not share a common mode of action. They act directly through their receptors on the IPCs, such as the CCHa2 receptor, the Sun receptor Methuselah or the TNF receptor Grindelwald (Agrawal et al., 2016; Delanoue et al., 2016; Sano, 2015). Alternatively, like in the case of Upd2, a neuronal relay is used (Rajan and Perrimon, 2012). In the case of the GBPs, the mechanism of action remains unknown (Koyama and Mirth, 2016).

Here, we report the identification of a short neural circuit required to adjust Dilp secretion in response to dietary amino acids, consisting in one pair of bilateral neurons making direct synaptic connections with the IPCs. Under low protein diet, these IPC-connecting neurons (ICNs) inhibit Dilp2 secretion. In fed larvae, ICNs activity is blocked, allowing Dilp release and animal growth. We further show that ICNs activity is controlled by fat-derived GBPs, which act as long-range hormonal agonists of EGFR signaling. In fed conditions, GBPs activate EGFR signaling in the ICNs, relieving their inhibitory effect on the IPCs and resulting in Dilp secretion. Altogether, our study reveals an unexpected role for EGF-like metabolic hormones and EGFR signaling as critical modulators of neural activity, coupling insulin secretion to the nutritional status.

Results

Identification of a pair of neurons contacting the IPCs

The IPCs are at the center of an elaborated network integrating various nutritional cues delivered in part by peripheral sensor tissues. In order to better characterize this intricate network, we first sought

to image the neuronal architecture of the IPCs. Using the IPC driver *dilp2-Gal4*, we expressed DenMark to visualize post-synaptic vesicles (Nicolai et al., 2010) and a Synaptotagmine::GFP (SyteGFP) fusion used as a presynaptic marker (Zhang et al., 2002). As previously described, we observed IPCs axons projecting towards the *Corpora cardiaca* (CC). More surprisingly, we could also observe a dense dendritic compartment surrounding the soma with branching running caudally along the midline through the subesophageal ganglion (SEG) (Figure 1A). This suggested that the IPCs receive inputs from afferent neurons connecting through their dendritic arborisations.

We then screened the *Janelia* neuronal GAL4 collection to identify driver lines expressing in neurons projecting towards the IPCs dendrites. We focused our attention on the *R22H11* line marking one pair of neurons located in the Pars Intercerebralis (PI) of the optic lobes, and one pair of CAPA-positive neurons in the posterior, ventral part of the medial subesophageal ganglion (CC-MS 2, Corpora Cardiaca-innervating neurosecretory neuron of the Medial Subesophageal ganglion 2) (Siegmund and Korge, 2001) (Figure S1). Interestingly, the *R22H11* PI neurons project their neurites towards the IPC dendrites (Figure 1B). By using the *dvGlut::GFP* fusion that marks presynaptic compartments (Riemensperger et al., 2013), we found that presynaptic vesicles of the *R22H11* PI neurons co-localize with the IPCs (Figure 1C). This suggests that *R22H11* neurons project axons towards the IPCs. Using the *GFP reconstitution across synaptic partners* (GRASP) (Feinberg et al., 2008) we could confirm direct contact between the two neuronal populations (Figure 1D). These findings therefore suggest that the *R22H11* PI neurons could directly contact the IPCs, and were named thereafter IPCs Connecting Neurons (ICNs).

The ICNs are inhibitory afferent neurons controlling IPC function.

To test whether the ICNs could functionally interfere with IPC secretory activity, we ablated the ICNs by expressing the pro-apoptotic gene *hid* with the *R22H11* driver (hereafter named *ICN-Gal4*). ICNs ablation induces pupal overgrowth (+15,6%) (Figure 2A and S2A) associated with a decrease in Dilp2 and Dilp5 staining in the IPCs (Figure 2C and S2G). We confirmed by Dilp2 ELISA (Park et al., 2014) that

reduced Dilp2 staining in the IPCs was the consequence of increased Dilp2 release in the hemolymph (Figure 2D). In line with this, pupal overgrowth is due to augmented growth rate (Figure 2E) with no effect on developmental timing (Figure S2C) or food intake (Figure S2D). Interestingly, when fed a **low protein diet (0,3x)**, *ICN>hid* larvae reach a body size nearly similar to control individuals (*ICN>w*) raised on rich protein diet (2x) (figure 2B), suggesting that animals with ablated ICNs are less responsive to amino acids in the diet. Both hyperpolarization of the ICNs using the potassic channel Kir2.1, or impaired secretion using tetanus toxin (TetX) led to pupal overgrowth, associated with reduced accumulation of Dilp2 and Dilp5 in the IPCs, and increased circulating Dilp2 levels (Figure 2A,C,D and Fig S2G). Converse experiments using the bacterial sodium channel NaChBac to induce chronic depolarization of the ICNs led to a strong reduction of circulating Dilp2 associated with accumulation of Dilp2 and Dilp5 in the IPCs (Figure 2C-D and S2G). However, in our experimental conditions, this was not sufficient to modify pupal volume (Figure 2A). In the same conditions, Dilp3 release was not modified (Figure S2H), consistent with the fact that Dilp3 levels are controlled by circulating sugars (Kim and Neufeld, 2015).

Importantly, no phenotype was observed using a *CAPA-Gal4* line expressed in the CAPA-positive subset of the *R22H11*-positive neurons (Figure S2B). This demonstrates that the ICNs located in the PI are sole responsible for the observed growth regulations. Since mRNA levels of *dilp2* or *dilp5* remain unchanged after manipulating ICNs activity (Figure S2E and F), we conclude that the ICNs are part of an inhibitory neural relay specifically acting on Dilp2 and Dilp5 secretion by the IPCs.

ICNs and IPCs present opposite responses to nutrition.

Our previous findings that IPCs modulate Dilp secretion according to nutritional cues (Geminard et al. 2009) and that ICN-ablated animals do not respond to low nutrient (Figure 2B) suggested that ICNs mediates the response to nutrition. The CaLexA reporter allows cumulative tracing of neuronal activity (Masuyama et al., 2012). Using this reporter, IPCs show a robust neuronal activity in fed conditions, which is abolished under amino acids starvation (Figure 3A). By contrast, ICNs exhibit basal activity in

fed conditions, which dramatically increases after acute amino acids starvation (Figure 3B). In addition, IPCs showed decreased activity at late wandering stage (a physiological state of cessation of feeding) compared to younger feeding larvae (Figure 3C), while ICNs activity strongly increases during this stage (Figure 3D). Therefore, IPCs and ICNs show opposite responses to nutrition, in line with the inhibitory action of ICNs on IPCs.

Ectopic expression of GBPs in the ICNs promotes body growth

We next tested whether ICNs could constitute a neuronal relay between the fat body and the IPCs in the nutritional response. To evaluate this possibility, we expressed various fat body-derived factors (FBS) in the ICNs and tested their possible autocrine action on ICNs function and animal growth. While Stunted or Unpaired 2 expression in the ICNs (*icn>sun*, *icn>upd2*) had no effect on pupal volume (Figure 4A, S3A-B), expression of GBP1 and GBP2 (*icn>gbp1*, *icn>gbp2*) led to pupal overgrowth similar to what obtained after GBP overexpression in the fat body (*lpp>gbp1*, *lpp>gbp2*) (Figure S3C). Like in the case of ICNs activity manipulation, this pupal overgrowth was coupled with increased Dilp2 secretion from the IPCs (Figure 4B). This autocrine response is specific for the ICNs since ectopic expression of GBPs in a neighboring neuronal population (*eh>gbp1*, *eh>gbp2*), or in the CAPA neurons targeted by the *R22H11* driver do not induce body growth increase (Figure S3D, S3E). These results indicate that ICNs respond to variations in GBPs levels to control Dilp release from the IPCs and systemic growth.

GBPs activate the EGFR signaling pathway

GBPs share 3-dimensional structure in their core region with EGF ligands (Aizawa et al., 2002) and bind to EGF receptor (EGFR) in human keratinocytes (Ohnishi et al., 2001). To better understand the mode of action of GBPs on ICNs, we first tested whether GBPs activate *Drosophila* EGFR signaling in insect cells. After activation by its ligands, EGFR dimerizes and undergoes auto-phosphorylation in trans on tyrosine. We therefore tested whether GBPs induce EGFR phosphorylation in co-cultured S2R+ cells

expressing EGFR::V5 and GBP1::HA as previously described (Lahusen et al., 2007) Anti-phosphotyrosine immunoprecipitation followed by anti-V5 western blotting indicates an increase of Tyr-phosphorylated EGFR::V5 in the presence of GBP1-HA (Figure 4C). This is accompanied by increased ERK phosphorylation (Figure 4D), as previously described (Tsuzuki et al., 2014). *In vivo*, ectopic expression of GBP1 in the posterior compartment of the wing imaginal disc (*hh>gbp1*) or in the wing pouch (*nub>gbp1*) increases phosphor-ERK levels in an autonomous manner (Figure 4E and 4F). This effect is abolished upon EGFR silencing (*nub>egfrRi, gbp1*) showing that GBP1 requires EGFR to activate ERK signaling *in vivo*. EGFR signaling controls wing vein patterning and, when in excess, leads to the formation of ectopic veins in the adult wing (Butchar et al., 2012). Ectopic expression of GBP1 or GBP2 in the wing pouch induces an extra vein phenotype (Figure 4G), confirming that both GBPs are potent activators of EGFR signaling *in vivo*. The wing vein phenotype is not detected when GBPs are produced from the adipose tissue (*lpp>GBP1*). This overall indicates that GBPs are potent activators of EGFR signaling both *in vitro* and *in vivo*. Moreover, fat-derived GBPs are able to mediate long range effects but do not interfere with EGFR signaling in imaginal tissues (Figure S3F).

EGFR signaling in the ICNs induces Dilps secretion and systemic growth

We next wondered whether GBPs action in the ICNs requires EGFR. For this, we first modified EGFR signaling in the ICNs and observed systemic growth effects. Inhibition of EGFR signaling in the ICNs (*icn>egfr-ri, icn>dsor-ri*) reduces pupal size (-8%) (Figure 5A and S4A), and Dilp2 release from the IPCs (Figure 5B). Conversely, increased EGFR signaling (*icn>egfr^{A887T}*) induces overgrowth (Figure 5A and S4A) and Dilp2 release (Figure 5B), while *dilp2* gene expression is unchanged (Figure S4B). Notably, no growth phenotype is observed when the *CAPA-GAL4* line is used to drive expression of the modified forms of EGFR (Figure S4C). Remarkably, overexpression of an activated form of Spitz (*icn>sspitz*) or its membrane tethered version (*icn>nrt::sspitz*) in the ICNs phenocopy GBP-induced growth (Figure S4D), but not overexpression of a non-processed form of Spitz (*icn>mspitz*, Figure S4D). This overall indicates that activation of EGFR in the ICNs is sufficient to promote systemic growth *via* Dilp release.

Although EGFR signaling could potentially impact cell proliferation, differentiation and migration (Shilo, 2003), we did not observe alteration in the number or the macroscopic organization of the ICNs in any of these conditions. In addition, ICNs with modified EGFR signaling still produce Tachykinin (dTK) (Figure S4E) and Myo-Inhibitory Peptide (MIP) (Figure S4E'), suggesting that their neuronal identity is not changed.

We further established that growth inhibition produced by reducing EGFR signaling in the ICNs (*icn>egfr-ri* or *icn>dsor-ri*) is epistatic to GBP1 overexpression (*icn>egfr ri; gbp1* or *icn>dsor ri; gbp1*) (Figure 5C,D, Figure S4F). This indicates that the GBPs exert their effect on the ICNs through activation of EGFR signaling. Altogether, these results indicate that GBPs produced by fat body cells in response to nutrients act remotely on the ICNs *via* EGFR signaling to promote systemic growth.

GBPs produced by fat cells repress ICNs activity through EGFR signaling.

We next tested whether GBP1 release from fat cells relies on dietary amino acids. For this, we generated a functional HA-tagged GBP1 allele. Its overexpression either in the fat body (*lpp>gbp1HA*) (Figure S5A) or in the ICNs (*icn>gbp1HA*) (Figure S5B) induces an overgrowth similar to that observed with unmodified GBP1. Upon acute amino acids starvation, we did not detect changes in GBP1::HA protein levels in adipose cells (*lpp>gbp1HA*), while hemolymph levels severely dropped (Figure 6A). Noticeably, in these conditions, fat body GBP1::HA-containing vesicles were enlarged compared to fed controls (Figure S5C). Importantly, using anti-HA antibody, we could detect fat-derived GBP1::HA decorating the ICNs of fed larvae (Figure 6F and S5D). These results indicate that the secretion of GBPs from fat cells is tightly controlled by nutrition, and that GBP1 molecules secreted by fat cells travel to the brain ICNs.

Since fat body derived-GBP1 has insulinotropic properties (Koyama and Mirth, 2016), we next assessed whether this effect is achieved *via* a relay using EGFR signaling in the ICNs. For this, hemolymph from control larvae (*lpp>w*) or larvae overexpressing *gbp1* in the fat body (*lpp>gbp1*) was collected to perform *ex vivo* brain culture experiments. When incubated with dissected control brains

(*icn>w*), hemolymph from *lpp>gbp1* larvae efficiently triggered Dilp2 secretion, confirming the insulinotropic function of GBPs. This effect was abolished upon EGFR silencing in the ICNs (*icn>egfr-ri*) brains (Figure 6B), indicating that fat body derived-GBP1 requires EGFR in the ICNs to stimulate Dilp2 secretion.

To better understand the function of GBP/EGFR signaling in ICNs, *icn>calexa* brains of wandering larvae were incubated with hemolymph collected from control larvae (*lpp>w*), larvae overexpressing *gbp1* in the fat body (*lpp>gbp1*) or larvae bearing a deletion of both *gbp1* and *gbp2* genes (*ex67^{-/-}*). While hemolymph from both control and *gbp1*-overexpressing larvae induced a decrease in ICNs neuronal activity, hemolymph from *ex67^{-/-}* mutant larvae had no effect (Figure 6C), demonstrating that circulating GBP1 represses ICNs neuronal activity. Similarly, overexpressing a constitutively activated form of EGFR in the ICNs (*calexa; icn>egfr^{A887T}*) efficiently repressed ICNs in wandering larvae (Figure 6D), while silencing EGFR (*calexa; icn>egfr-ri*) activated them in L3 larvae (Figure 6E). Hence, we conclude from these data that activation of EGFR signaling by circulating GBPs inhibits ICNs neuronal activity, therefore releasing ICNs-mediated inhibition of the IPCs.

Discussion

EGFR signaling exerts a central control on cell growth and differentiation, and as such is essential in multiple developmental processes. Our study proposes a new paradigm for EGFR signaling by establishing that EGF receptor and its atypical GBP ligands play a pivotal role in controlling neuronal activity and, as a consequence, adapt the rate of tissue growth according to nutritional cues.

GBPs act as long-distance EGFR ligands.

RMN analysis suggests that the core region of GBPs has structural similarity with the C-terminal domain of EGF (Aizawa et al., 1999, 2002). Several experimental approaches provided conclusive evidence of direct binding of GBPs to EGFR in keratinocytes, other results suggested that unidentified receptor and co-receptor or adaptor protein might exist in insect cells (Aizawa et al., 2002; Oda et al.,

2010; Ohnishi et al., 2001). More recently, GBPs were proposed to interact with the GPCR Mthl10, but there is no direct evidence that this interaction has functional significance for the control of IPCs function (Sung et al., 2017).

Our study establishes that *gbp1* overexpression can efficiently stimulate EGFR-dependent signaling, both in cultured cells and in developing organs. We also provide genetic evidence that the function of fat body derived-GBPs in controlling Dilp secretion entirely relies on the presence of EGFR in the ICNs.

In both mammals and flies, several ligands activate EGFR signaling to fulfill a variety of biological responses (Ceresa and Peterson, 2014). The main ligand for EGFR, Spitz, is palmitoylated, which reduces its secretion and its range of action (Miura et al., 2006). By contrast, we show that GBPs produced by the fat body can travel over long distances and bind to the brain ICNs, therefore providing a signal for inter-organ communication (see Figure 6F and S5D). We do not know how GBPs are processed, secreted by adipose tissue and transported in the hemolymph. It is possible that fat body-derived GBPs acquire distinct features, such as post-translational modifications, association with co-partners, packaging, required to signal over long distance. These specific features, or the localization of EGFR at the surface of imaginal epithelia could explain why adipose GBP does not activate EGFR in imaginal tissues. Similarly, Hedgehog (Hh) produced by the larval gut circulates in the hemolymph associated with lipoprotein particles and modifies animal growth rate and developmental timing, with no effect on imaginal Hh signaling (Rodenfels et al., 2014). Recent data suggest that mammalian EGF-like ligands with endocrine function could be packed into signaling competent exosomes (Singh et al., 2016).

The mechanisms of GBP released into the hemolymph is uncharacterized. However, we show that GBP secretion is highly dependent on the nutritional status, since HA-tagged GBP1, although highly produced in fat cells under an ectopic Gal4 system, is undetectable in the hemolymph when larvae are subjected to amino acids starvation. TORC1 signaling controls *gbp* gene transcription (Koyama and

Mirth, 2016). It will be interesting to know whether GBP secretion is also controlled by TORC1 activity or by alternative pathways.

EGFR function in the ICNs

In the CNS, EGFR and its various ligands promote differentiation, maturation and survival of a variety of neurons (Wong and Guillaud, 2004). In the present work, we observed that EGFR signaling in the ICNs is not needed for their architecture or their neuronal identity. Surprisingly, activation of EGFR reduces intracellular calcium and represses ICNs activity. Other pathways than MAPK signaling could be activated downstream of EGFR, such as PI3K/AKT or phospholipase-C γ (PLC- γ), which could promote intracellular calcium release. These branches of EGFR signaling control cell migration and invasion (Wee and Wang, 2017). However, in the context of ICNs, activation of EGFR leads to calcium decrease, and we found that dSOR, one downstream component of the MAPK pathway, is involved in this process. Interestingly, components of MAPK signaling are present in distal neural structures such as dendrites and synapses, suggesting that this pathway is not limited to the regulation of gene expression and can control local synaptic activity in a more acute manner. Indeed, several synaptic proteins have been identified as ERK/MAPK substrates such as scaffolding PSD proteins, Kv4.2 potassium channels or group I metabotropic glutamate receptors (Schrader et al., 2006). Phosphorylation of these components by ERK/MAPK modifies their trafficking and synaptic delivery and thus determines the strength and the efficacy of excitatory synapses (Mao and Wang, 2016). These would be interesting targets for a role of EGFR in ICNs to evaluate in future studies.

A general mechanism for Insulin-like peptide secretion.

Interestingly, non-autonomous control of ILP secretion by EGF/EGFR signaling has recently been described in the fly developing brain. Here, an EGF-like ligand produced by the photoreceptors stimulates the production of the Insulin-like peptide Dilp6 in adjacent glial cells, and this process is required for lamina neuronal differentiation (Fernandes et al., 2017). In mammals, amino acids have

insulinotropic effects and deficiencies in dietary proteins are associated with impaired insulin secretion (Newsholme et al., 2007; Zhang and Li, 2013). One possible mechanism for this regulation could involve a central relay through direct innervation of the pancreatic islets (Horiuchi et al., 2017; Rosario et al., 2016). In addition, EGF ligands can stimulate insulin release from pancreatic islets (Lee et al., 2008). However, it is not clear what tissue could be producing the EGF signal in such regulation. Therefore, the present work gives a prospect for further studies identifying key circuitries required for insulin/IGF secretion.

Acknowledgements

We thank Alessandra Mauri, Gisèle Jarretou and Thomas Phil for technical assistance. We thank all members of the laboratory for insightful discussions and comments on the manuscript. We thank the Vienna *Drosophila* RNAi Center, the *Drosophila* Genetics Resource Center (NIH grant: 2P40OD010949), the Bloomington stock Center for providing *Drosophila* lines. This work was supported by the CNRS, INSERM, European Research Council (Advanced grant no. 268813 to P.L.), ARC (grant n° PGA120150202355 to P.L.), the Labex Signallife program (grant ANR-11-LABX-0028-01 to P.L.), the French government (PhD fellowship to E.M.) and the Fondation pour la Recherche Médicale (FDT20170437244 PhD fellowship to E.M.).

Authors Contributions

Conceptualization: RD and PL, Methodology: RD and PL, Formal analysis: EM, Investigation: EM and RD, Writing original draft: RD, EM and PL, Writing review & editing: RD, EM and PL, Visualization: EM, Supervision: RD and PL, Project Administration: RD and PL, Funding acquisition: PL.

Declaration of Interests

The authors declare no competing interests.

References

- Agrawal, N., Delanoue, R., Mauri, A., Basco, D., Pasco, M., Thorens, B., and Léopold, P. (2016). The *Drosophila* TNF Eiger Is an Adipokine that Acts on Insulin-Producing Cells to Mediate Nutrient Response. *Cell Metab.* *23*, 675–684.
- Aizawa, T., Fujitani, N., Hayakawa, Y., Ohnishi, A., Ohkubo, T., Kumaki, Y., Kawano, K., Hikichi, K., and Nitta, K. (1999). Solution structure of an insect growth factor, growth-blocking peptide. *J. Biol. Chem.* *274*, 1887–1890.
- Aizawa, T., Hayakawa, Y., Nitta, K., and Kawano, K. (2002). Structure and activity of insect cytokine GBP which stimulates the EGF receptor. *Mol. Cells* *14*, 1–8.
- Azpiaz, N., and Morata, G. (2000). Function and regulation of homothorax in the wing imaginal disc of *Drosophila*. *Development* *127*, 2685 LP-2693.
- Brankatschk, M., and Eaton, S. (2010). Lipoprotein Particles Cross the Blood–Brain Barrier in *Drosophila*; *J. Neurosci.* *30*, 10441 LP-10447.
- Brankatschk, M., Dunst, S., Nemetschke, L., and Eaton, S. (2014). Delivery of circulating lipoproteins to specific neurons in the *Drosophila* brain regulates systemic insulin signaling. *Elife* *3*, e02862.
- Brogio, W., Stocker, H., Ikeya, T., Rintelen, F., Fernandez, R., and Hafen, E. (2001). An evolutionarily conserved function of the *Drosophila* insulin receptor and insulin-like peptides in growth control. *Curr. Biol.* *11*, 213–221.
- Burke, R., Nellen, D., Bellotto, M., Hafen, E., Senti, K.-A., Dickson, B.J., and Basler, K. (1999). Dispatched, a Novel Sterol-Sensing Domain Protein Dedicated to the Release of Cholesterol-Modified Hedgehog from Signaling Cells. *Cell* *99*, 803–815.
- Butchar, J.P., Cain, D., Manivannan, S.N., McCue, A.D., Bonanno, L., Halula, S., Truesdell, S., Austin, C.L., Jacobsen, T.L., and Simcox, A. (2012). New negative feedback regulators of Egfr signaling in *Drosophila*. *Genetics* *191*, 1213–1226.
- Ceresa, B.P., and Peterson, J.L. (2014). *Cell and Molecular Biology of Epidermal Growth Factor Receptor* (Elsevier Inc.).
- Colombani, J., Raisin, S., Pantalacci, S., Radimerski, T., Montagne, J., and Léopold, P. (2003). A nutrient sensor mechanism controls *Drosophila* growth. *Cell* *114*, 739–749.
- Colombani, J., Andersen, D.S., and Léopold, P. (2012). Secreted peptide Dilp8 coordinates *Drosophila* tissue growth with developmental timing. *Science* *336*, 582–585.
- Delanoue, R., Meschi, E., Agrawal, N., Mauri, A., Tsatskis, Y., McNeill, H., Leopold, P., and Léopold, P. (2016). *Drosophila* insulin release is triggered by adipose Stunted ligand to brain Methuselah receptor. *Science* (80-.). *353*, 1553–1556.
- Delanoue, R.R., Slaidina, M., and Léopold, P. (2010). The steroid hormone ecdysone controls systemic growth by repressing dMyc function in *drosophila* fat cells. *Dev. Cell* *18*, 1012–1021.
- Donadon, V., Balbi, M., and Zanette, G. (2009). Hyperinsulinemia and risk for hepatocellular carcinoma in patients with chronic liver diseases and Type 2 diabetes mellitus. *Expert Rev. Gastroenterol. Hepatol.* *3*, 465–467.
- Feinberg, E.H., VanHoven, M.K., Bendesky, A., Wang, G., Fetter, R.D., Shen, K., and Bargmann, C.I. (2008). GFP Reconstitution Across Synaptic Partners (GRASP) Defines Cell Contacts and Synapses in Living Nervous Systems. *Neuron* *57*, 353–363.
- Fernandes, V.M., Chen, Z., Rossi, A.M., Zipfel, J., and Desplan, C. (2017). Glia relay differentiation cues to coordinate neuronal development in *Drosophila*. *Science* (80-.). *357*, 886 LP-891.
- Garofalo, R.S. (2002). Genetic analysis of insulin signaling in *Drosophila*. *Trends Endocrinol. Metab.* *13*, 156–162.
- Géminard, C., Rulifson, E.J., and Léopold, P. (2009). Remote control of insulin secretion by fat cells in *Drosophila*. *Cell Metab.* *10*, 199–207.
- Hayakawa, Y. (1991). Structure of a growth-blocking peptide present in parasitized insect hemolymph. *J. Biol. Chem.* *266*, 7982–7984.
- Hayakawa, Y., and Ohnishi, A. (1998). Cell Growth Activity of Growth-Blocking Peptide. *Biochem. Biophys. Res. Commun.* *250*, 194–199.
- Hombria, J.C.-G., Brown, S., Häder, S., and Zeidler, M.P. (2005). Characterisation of Upd2, a *Drosophila* JAK/STAT pathway ligand. *Dev. Biol.* *288*, 420–433.
- Horiuchi, M., Takeda, T., Takanashi, H., Ozaki-Masuzawa, Y., Taguchi, Y., Toyoshima, Y., Otani, L., Kato, H., Sone-Yonezawa, M., Hakuno, F., et al. (2017). Branched-chain amino acid supplementation restores reduced insulinotropic activity of a low-protein diet through the vagus nerve in rats. *Nutr. Metab.* *14*, 1–12.
- Ikeya, T., Galic, M., Belawat, P., Nairz, K., and Hafen, E. (2002). Nutrient-dependent expression of insulin-like peptides from neuroendocrine cells in the CNS contributes to growth regulation in *Drosophila*. *Curr. Biol.* *12*,

1293–1300.

- Kean, L., Cazenave, W., Costes, L., Broderick, K.E., Graham, S., Pollock, V.P., Davies, S.A., Veenstra, J.A., and Dow, J.A.T. (2002). Two nitridergic peptides are encoded by the gene capability in *Drosophila melanogaster*. *Am. J. Physiol. Integr. Comp. Physiol.* *282*, R1297–R1307.
- Kim, J., and Neufeld, T.P. (2015). Dietary sugar promotes systemic TOR activation in *Drosophila* through AKH-dependent selective secretion of Dilp3. *Nat. Commun.* *6*, 6846.
- Koyama, T., and Mirth, C.K. (2016). Growth-Blocking Peptides As Nutrition-Sensitive Signals for Insulin Secretion and Body Size Regulation. *PLOS Biol.* *14*, e1002392.
- Lahusen, T., Fereshteh, M., Oh, A., Wellstein, A., and Riegel, A.T. (2007). Epidermal Growth Factor Receptor Tyrosine Phosphorylation and Signaling Controlled by a Nuclear Receptor Coactivator, Amplified in Breast Cancer 1. *Cancer Res.* *67*, 7256–7265.
- Lee, H.Y., Yea, K., Kim, J., Lee, B.D., Chae, Y.C., Kim, H.S., Lee, D.W., Kim, S.H., Cho, J.H., Jin, C.J., et al. (2008). Epidermal growth factor increases insulin secretion and lowers blood glucose in diabetic mice. *J. Cell. Mol. Med.* *12*, 1593–1604.
- Liu, Y., Liao, S., Veenstra, J.A., and Nässel, D.R. (2016). *Drosophila* insulin-like peptide 1 (DILP1) is transiently expressed during non-feeding stages and reproductive dormancy. *Sci. Rep.* *6*, 1–15.
- Mao, L.-M., and Wang, J.Q. (2016). Regulation of Group I Metabotropic Glutamate Receptors by MAPK/ERK in Neurons. *J. Nat. Sci.* *2*, 1–8.
- Masuyama, K., Zhang, Y., Rao, Y., and Wang, J.W. (2012). Mapping Neural Circuits with Activity-Dependent Nuclear Import of a Transcription Factor. *J. Neurogenet.* *26*, 89–102.
- McNabb, S.L., Baker, J.D., Agapite, J., Steller, H., Riddiford, L.M., and Truman, J.W. (1997). Disruption of a Behavioral Sequence by Targeted Death of Peptidergic Neurons in *Drosophila*. *Neuron* *19*, 813–823.
- Miura, G.I., Buglino, J., Alvarado, D., Lemmon, M. a, Resh, M.D., and Treisman, J.E. (2006). Palmitoylation of the EGFR ligand Spitz by Rasp increases Spitz activity by restricting its diffusion. *Dev. Cell* *10*, 167–176.
- Newsholme, P., Bender, K., Kiely, A., and Brennan, L. (2007). Amino acid metabolism, insulin secretion and diabetes. *Biochem. Soc. Trans.* *35*, 1180–1186.
- Nicolai, L.J.J., Ramaekers, A., Raemaekers, T., Drozdzecki, A., Mauss, A.S., Yan, J., Landgraf, M., Annaert, W., and Hassan, B.A. (2010). Genetically encoded dendritic marker sheds light on neuronal connectivity in *Drosophila*. *Proc. Natl. Acad. Sci.* *107*, 20553–20558.
- Oda, Y., Matsumoto, H., Kurakake, M., Ochiai, M., Ohnishi, A., and Hayakawa, Y. (2010). Adaptor protein is essential for insect cytokine signaling in hemocytes. *Proc. Natl. Acad. Sci. U. S. A.* *107*, 15862–15867.
- Ohnishi, A., Oda, Y., and Hayakawa, Y. (2001). Characterization of Receptors of Insect Cytokine, Growth-blocking Peptide, in Human Keratinocyte and Insect Sf9 Cells. *J. Biol. Chem.* *276*, 37974–37979.
- Park, S., Alfa, R.W., Topper, S.M., Kim, G.E.S., Kockel, L., and Kim, S.K. (2014). A genetic strategy to measure circulating *Drosophila* insulin reveals genes regulating insulin production and secretion. *PLoS Genet.* *10*, e1004555.
- Pfeiffer, B.D., Ngo, T.-T.B., Hibbard, K.L., Murphy, C., Jenett, A., Truman, J.W., and Rubin, G.M. (2010). Refinement of tools for targeted gene expression in *Drosophila*. *Genetics* *186*, 735–755.
- Rajan, A., and Perrimon, N. (2012). *Drosophila* cytokine unpaired 2 regulates physiological homeostasis by remotely controlling insulin secretion. *Cell* *151*, 123–137.
- Riemensperger, T., Issa, A.R., Pech, U., Coulom, H., Nguyễn, M.V., Cassar, M., Jacquet, M., Fiala, A., and Birman, S. (2013). A Single Dopamine Pathway Underlies Progressive Locomotor Deficits in a *Drosophila* Model of Parkinson Disease. *Cell Rep.* *5*, 952–960.
- Rodenfels, J., Lavrynenko, O., Ayciriex, S., Sampaio, J.L., Carvalho, M., Shevchenko, A., and Eaton, S. (2014). Production of systemically circulating Hedgehog by the intestine couples nutrition to growth and development. *Genes Dev.* *28*, 2636–2651.
- Rosario, W., Singh, I., Wautlet, A., Patterson, C., Flak, J., Becker, T.C., Ali, A., Tamarina, N., Philipson, L.H., Enquist, L.W., et al. (2016). The brain-to-pancreatic islet neuronal map reveals differential glucose regulation from distinct hypothalamic regions. *Diabetes* *65*, 2711–2723.
- Rulifson, E.J., Kim, S.K., and Nusse, R. (2002). Ablation of insulin-producing neurons in flies: growth and diabetic phenotypes. *Science* *296*, 1118–1120.
- Sano, H. (2015). Coupling of growth to nutritional status: The role of novel periphery-to-brain signaling by the CCHa2 peptide in *Drosophila melanogaster*. *Fly (Austin)*. *9*, 183–187.
- Sano, H., Nakamura, A., Texada, M.J., Truman, J.W., Ishimoto, H., Kamikouchi, A., Nibu, Y., Kume, K., Ida, T., and Kojima, M. (2015). The Nutrient-Responsive Hormone CCHamide-2 Controls Growth by Regulating Insulin-like Peptides in the Brain of *Drosophila melanogaster*. *PLoS Genet.* *11*, 1–26.
- Schrader, L.A., Birnbaum, S.G., Nadin, B.M., Ren, Y., Bui, D., Anderson, A.E., and Sweatt, J.D. (2006). ERK/MAPK

regulates the Kv4.2 potassium channel by direct phosphorylation of the pore-forming subunit. *Am. J. Physiol. Physiol.* **290**, C852–C861.

Schweitzer, R., Shaharabany, M., and Seger, R. (1995). Secreted Spitz triggers the DER signaling pathway and is a hmltmg component in embryonic ventral ectoderm determination. *Genes Dev.* **15**, 1518–1529.

Shilo, B. (2003). Signaling by the *Drosophila* epidermal growth factor receptor pathway during development. *Exp. Cell Res.* **284**, 140–149.

Siegmund, T., and Korge, G. (2001). Innervation of the ring gland of *Drosophila melanogaster*. *J. Comp. Neurol.* **431**, 481–491.

Singh, B., Carpenter, G., and Coffey, R.J. (2016). EGF receptor ligands: recent advances. *F1000Research* **5**, 2270.

Slaidina, M., Delanoue, R., Gronke, S., Partridge, L., and Léopold, P. (2009). A *Drosophila* Insulin-like Peptide Promotes Growth during Nonfeeding States. *Dev. Cell* **17**, 874–884.

Steinhauer, J., Liu, H.H., Miller, E., and Treisman, J.E. (2013). Trafficking of the EGFR ligand Spitz regulates its signaling activity in polarized tissues. *J. Cell Sci.* **126**, 4469–4478.

Sung, E.J., Ryuda, M., Matsumoto, H., Uryu, O., Ochiai, M., Cook, M.E., Yi, N.Y., Wang, H., Putney, J.W., Bird, G.S., et al. (2017). Cytokine signaling through *Drosophila* Mthl10 ties lifespan to environmental stress. *Proc. Natl. Acad. Sci.*

Tanimoto, H., Itoh, S., ten Dijke, P., and Tabata, T. (2000). Hedgehog Creates a Gradient of DPP Activity in *Drosophila* Wing Imaginal Discs. *Mol. Cell* **5**, 59–71.

Tsruya, R., Schlesinger, A., Reich, A., Gabay, L., Sapir, A., and Shilo, B.-Z. (2002). Intracellular trafficking by Star regulates cleavage of the *Drosophila* EGF receptor ligand Spitz. *Genes Dev.* **16**, 222–234.

Tsuzuki, S., Matsumoto, H., Furihata, S., Ryuda, M., Tanaka, H., Jae Sung, E., Bird, G.S., Zhou, Y., Shears, S.B., and Hayakawa, Y. (2014). Switching between humoral and cellular immune responses in *Drosophila* is guided by the cytokine GBP. *Nat. Commun.* **5**, 1–11.

Veenstra, J.A., Agricola, H.-J., and Sellami, A. (2008). Regulatory peptides in fruit fly midgut. *Cell Tissue Res.* **334**, 499–516.

Wee, P., and Wang, Z. (2017). Epidermal growth factor receptor cell proliferation signaling pathways. *Cancers (Basel)*. **9**, 1–45.

Witek, G., Verhaert, P., Lorenz, M.W., and Hoffmann, K.H. (1999). Immunolocalization of two types of allatostatins in the central nervous system of the cricket *Gryllus bimaculatus* (Ensifera: Gryllidae). *Eur. J. Entomol.* **96**, 279–285.

Wong, R.W.C., and Guillaud, L. (2004). The role of epidermal growth factor and its receptors in mammalian CNS. *Cytokine Growth Factor Rev.* **15**, 147–156.

Zhang, T., and Li, C. (2013). Mechanisms of amino acid-stimulated insulin secretion in congenital hyperinsulinism. *Acta Biochim. Biophys. Sin. (Shanghai)*. **45**, 36–43.

Zhang, Y.Q., Rodesch, C.K., and Broadie, K. (2002). Living synaptic vesicle marker: Synaptotagmin-GFP. *Genesis* **34**, 142–145.

Figure Legends

Figure 1: *R22H11* neurons present axonal projections making physical contacts with the IPCs

(A) *UAS-DenMark*; *UAS-SytcGFP* are driven by the IPCs driver, *dilp2-GAL4*. The dendritic marker DenMark is used to visualize the IPCs dendrites (red), and SytcGFP reveals their axonal architecture (green).

(B) The *R22H11-GAL4* line drives *mCD8GFP* (green) in one neuron in each brain hemisphere, sending projections towards the IPCs (anti-Dilp2, red) (hereafter referred as ICNs, see text).

(C) Expression of *UAS-DVglt::GFP* (a vesicular transporter of glutamate) driven by *R22H11-GAL4* (hereafter referred to as *icn-Gal4*) labels presynaptic vesicles (green). Analysis of z sections reveals that ICNs axons (green) co-localize with the IPCs (anti-Dilp2, red) along their neuronal tracts and cell bodies.

(D) GFP reconstitution across synaptic partners (GRASP) shows physical connections between IPCs and ICNs. *icn-LexA* and *dilp2-GAL4* are used to express membrane-tethered split-GFP *LexAop-CD4::spGFP11* and *UAS-CD4::spGFP1-10*, respectively. IPCs are stained by the anti-Dilp2 (cyan) and ICNs are labeled with a membrane associated RFP (dsRed, red). The GRASP signal is visualized in green.

CC: Corpora Cardiaca SEG: Subesophageal ganglion

See also Figure S1.

Figure 2: ICNs inhibit body growth by blocking Dilps secretion

(A) Pupal volume measurement after ICNs ablation (*icn>hid*), hyperpolarization (*icn>kir2.1*), blockade of secretory activity (*icn>tetx*) or chronic depolarization (*icn>nachbac*). (n≥238)

(B) Pupal volume measurement after ICNs ablation (*icn>hid*) in high protein diet (2x) and low protein diet (0,3x). (n≥75)

(C) Dilp2 accumulation levels in the IPCs upon ICNs ablation (*icn>hid*), hyperpolarization (*icn>kir2.1*) secretion blockade (*icn>tetx*) or depolarization (*icn>nachbac*). (n≥62) Fluorescence intensity is measured as delta ratio compared to control (*icn>w*).

(D) ELISA test of Dilp2HF (*gd2HF*) circulating levels in the hemolymph upon ICNs ablation (*icn>hid*), hyperpolarization (*icn>kir2.1*), secretion blockade (*icn>tetx*) or depolarization (*icn>nachbac*). (n≥4 for 3 independent experiments)

(E) Larval growth curve after ICNs ablation (*icn>hid*), compared to controls (*icn>w* and *w hid*). (n≥57).

In all graphs, means are shown and errors bars represent ±SEM, ****p<0,0001, **p<0,01, *p<0,05.

See also Figure S2.

Figure 3: IPCs and ICNs show antagonistic regulation by nutrition and developmental stage

A. Analysis of IPCs neuronal activity in fed and starved (1% sucrose) conditions using the calcium reporter *UAS-CaLexA* crossed with *dilp2-Gal4*. (n≥68)

B. Analysis of ICNs neuronal activity in fed and starved (1% sucrose) conditions using the calcium reporter *UAS-CaLexA* crossed with *icn-Gal4*. (n≥56)

C. Analysis of IPCs neuronal activity at 80h AEL and 120h AEL (wandering stage) using the calcium reporter *UAS-CaLexA* crossed with *dilp2-Gal4*. (n≥48)

D. Analysis of ICNs neuronal activity at 80h AEL and 120h AEL (wandering stage) using the calcium reporter *UAS-CaLexA* crossed with *icn-Gal4*. (n≥69)

In graphs, means are shown and errors bars represent ±SEM, ****p<0,0001.

Figure 4: Growth-Blocking-Peptides (GBPs) are putative EGF ligands inducing systemic body growth when expressed in the ICNs

- A. Ectopic expression of *gbp1* or *gbp2* in the ICNs (*icn>gbp1* and *icn>gbp2*) leads to increased pupal volume. (n≥408)
- B. Dilp2 signal in IPCs decreases upon *gbp1* and *gbp2* ectopic expression in ICNs. (n≥34)
- C. GBP1 induces tyrosine auto-phosphorylation of EGFR in S2 cells (co-culture of GBP1::HA expressing cells with EGFR::V5 expressing cells, immunoprecipitation with anti-phospho-Tyr antibodies, western blotting using anti-V5 antibody).
- D. Co-culture of EGFR::V5 expressing cells with either GBP1- or GBP2-expressing cells tested for ERK phosphorylation (pERK). The EGFR ligand Spitz (cSpi::GFP) and Hedgehog-HA (Hh::HA) are used as positive and negative controls, respectively.
- E. ERK phosphorylation (pERK) induction upon ectopic *gbp1* expression in the Hedgehog expressing domain of the wing pouch (*hh>mcherry; gbp1*).
- F. ERK phosphorylation (pERK) observed upon ectopic *gbp1* expression in the wing pouch (*nub>gbp1*) requires EGFR (*nub>egfrRi, gbp1*).
- G. Ectopic *gbp1* and *gbp2* expression in the wing pouch using *nub-GAL4* driver (*nub>gbp1* and *nub>gbp2*) induce extra veins (L2) (n≥51).

In graphs, means are shown and errors bars represent \pm SEM, ****p<0,0001.

See also Figure S3.

Figure 5: GBP1 in the ICNs promotes body growth through EGFR signaling pathway

- A. Pupal volumes after silencing *egfr* (*icn>egfrRi*) or *dsor*, (*icn>dsorRi*) or activating EGFR signaling (*icn>egfr^{A887T}*) in ICNs. (n≥83)
- B. IPCs-Dilp2 retention after silencing *egfr* (*icn>egfrRi*) or *dsor*, (*icn>dsorRi*) or activating EGFR signaling (*icn>egfr^{A887T}*) in ICNs. (n≥58)
- C. Pupal volumes after ectopic expression of *gbp1* alone (*icn>gbp1*), or upon co-silencing EGFR (*icn>egfrRi, gbp1*) in the ICNs. (n≥77)
- D. IPCs-Dilp2 accumulation after ectopic expression of *gbp1* alone (*icn>gbp1*), or upon co-silencing EGFR (*icn>egfrRi, gbp1*) in the ICNs. (n≥57)

In graphs, means are shown and errors bars represent \pm SEM, ****p<0,0001.

See also Figure S4.

Figure 6: Fat body-derived GBP1 is secreted in the hemolymph and acts on ICNs neuronal activity through EGFR

- A. Western blotting experiment (anti-HA) on hemolymph extracts and dissected fat bodies from *lpp>gbp1::HA* larvae in either fed or acute amino acids starvation state.
- B. Brain culture with hemolymph collected from control larvae or larvae overexpressing *gbp1* in the fat body (*lpp>gbp1*) tested for IPC-Dilp2 retention. Brains were extracted from either *icn>w* control or *icn>egfrRi* animals. (n≥48)
- C. Brain culture with hemolymph collected from control larvae, larvae overexpressing *gbp1* in the fat body (*lpp>gbp1*) or larvae deficient for *gbp1* and *gbp2* (*ex67^{-/-}*) tested for ICNs neuronal activity using the CaLexA calcium marker (*icn>calexa*). (n≥47)
- D. The CaLexA reporter is used to test ICNs activity upon constitutive active EGFR expression (*icn>calexA, egfr^{A887T}*) at late wandering stage (123h. AEL). (n≥44)
- E. The CaLexA reporter is used to test ICNs activity upon silencing EGFR expression (*icn>calexA, egfrRi*) during L3 feeding stages (96h. AEL). (n≥33)
- F. GBP1::HA (green) specifically expressed in the fat body (*lpp>gbp1::HA*) is detected in the ICNs, labelled with an anti-Tachykinine (dTK, red) antibody.

In graphs, means are shown and errors bars represent \pm SEM, ****p<0,0001, **p<0,01.

See also Figure S5.

STAR Methods

Contact for reagent and resource sharing

Further information and requests for resources and reagents should be directed to and will be fulfilled by the Lead Contact, Pierre Léopold (pierre.leopold@curie.fr).

Experimental model and Subject Details

Fly strains and maintenance

The following fly strains were used: white¹¹¹⁸ (*w*), *dilp2-GAL4* (Rulifson et al., 2002), *hh-GAL4* (Tanimoto et al., 2000), *nubbin-GAL4* (Azpiazu and Morata, 2000), *lpp-GAL4* (gift from S. Eaton), *lexAop-CD8-GFP-2A-CD8-GFP*; *UAS-mLexA-VP16-NFAT*, *LexAop-rCD2-GFP* (gift from Jing W. Wang), *UAS-dvglut::GFP* (gift from S. Birman), *UAS-sun* (gift from W Ja), *UAS-upd2* (gift from N. Perrimon). K. Mirth and T. Koyama kindly provided the following lines: *UAS-gbp1*, *UAS-gbp2*, *ex67^{-/-}*. The *UAS-mspi*, *UAS-sspi* and *UAS-nrt::sspi* strains were a kind gift by J. Treisman.

R22H11-GAL4 (RRID:BDSC 48043) (Pfeiffer et al., 2010) and *R22H11-LexA* (RRID:BDSC_54109) lines come from Janelia Farm (BDSC).

RNAi lines come from the Vienna Drosophila RNAi Stock Center: *UAS-egfrRi* (107130KK), *UAS-dsorRi* (107276KK).

UAS-hid; *UAS-tetx*; *UAS-kir2.1*; *UAS-NaChBac*; *UAS-egfr^{A887T}*; *EH-GAL4* (C21); *UAS-mCD8-GFP*; *UAS-mcherry*; *CAPA-GAL4*; *UAS-DenMark*, *UAS-syteGFP* and *lexAop-rCD2-RFP*; *UAS-CD4-spGFP1-10*, *lexAop-CD4-spGFP11* were provided by the Bloomington Drosophila Stock Center.

Animals were reared at 25°C on fly food containing per liter, 10g of agar, 83g corn flour, 60g white sugar, 34g dry yeast and 3,75g Moldex (diluted in ethanol). For all experiments, both males and females have been used.

In Fig1 and S1, wandering larvae were dissected. Pupae were measured at day 2 after pupariation. Dilp2 and Dilp5 stainings were done on L3 larvae (96 hours after egg laying). The CaLexA experiments were made on L3 or wandering larvae, depending on the condition (explained on each figure legend). Wings were collected at day 1 after adult emergence. Wing discs from wandering larvae were stained. Hemolymph and fat bodies for western blots were collected from L3 larvae (96 hours after egg laying). Brains of L3 larvae (96 hours after egg laying) were used for qPCR experiments. Feeding behavior assay was done on L3 larvae (96 hours after egg laying).

Cell culture

S2R+ cells were maintained in Schneider medium supplemented with 10% FBS and 1% streptomycin at 22°C. All UAS plasmids were co-transfected with *actin-GAL4* using lipofectamine (ThermoFisher Scientific).

Method Details

Plasmids and generation of transgenic lines

gfp1 and *gfp2* coding sequences were PCR amplified from DGRC cDNA clones IP05665 and GH14572 respectively. They were cloned into the pENTR/D-TOPO vector using the following gene-specific primers: sense primer CAC CGA ATT CAG GAT GTT GAT ACG TAT TAA TCC ATT GGT G and antisense primer CCG GAA TTC CGC CGG CTT TCT GCA TCG TTT TCC for *gfp1* and sense primer CAC CGG TAC CAG GAT GTT TTT GCA ACT CTT ATC TAT A and antisense primer CCG GGT ACC GGC TTC CTT CCT GCA ACG TCC TGC for *gfp2*. To generate the *UAS-gfp1::HA* and *UAS-gfp2::HA* lines, coding sequences were cloned into the Gateway Destination vector (Drosophila Gateway Vector Collection) the pTWH.

UAS-gbp1::HA construct was then introduced into the germ line by injections in *w¹¹¹⁸* fly line (BestGene).

pBDP2 gdilp2-BHA-FLAGA (gift from S. K. Kim) was injected in the Bloomington stock #24484 to generate a new *y¹ w¹¹¹⁸; gd2HF(attP2)*. J. Treisman kindly provided the *mt-egfr::V5* and *UAS-cSpi::GFP* plasmids. *UAS-hh::HA* was kindly provided by K. Basler.

Fly Media

Our experiments are usually performed on a rich protein diet containing per liter, 10g of agar, 83g corn flour, 60g white sugar, 34g dry yeast and 3,75g Moldex (diluted in ethanol). The low protein diet or 0,3x media used in Figure 2B contains per liter, 10g of agar, 83g corn flour, 60g white sugar, 5g dry yeast and 3,75g Moldex (diluted in ethanol).

Amino acids starvation

72h AEL larvae are transferred for 16h on PBS 1x, 2% agar plates and supplemented with 1% sugar, but no protein source.

Feeding behavior

Blue food dye (Erioglaucine Disodium Salt, Sigma-Aldrich) was added at 1,5% in the food. Larvae were left in blue food for 3 hours at 25°C, washed, put in microtubes (8 larvae per tube), and frozen. Samples were homogenized in water and spun down for 5 min at 13000 rpm, and the amount of blue dye in the supernatant was measured by spectrophotometry (OD₆₂₉ Nanovue). *n* represents biological replicates. For a given experiment all values are normalized to one single condition.

Pupal volume analysis

Larvae were synchronized at 24h AED and reared under controlled conditions (30 larvae/vial). Pupal volume was measured using ImageJ and calculated by using the formula

$$\frac{4}{3} * \pi * \left(\frac{length}{2}\right) * \left(\frac{width}{2}\right)^2$$

n represents pupae number. For a given experiment, all values are normalized to one control condition to give the “Δ pupal volume ratio”.

Ex vivo Organ culture

We performed ex vivo organ culture as described in (Géminard et al., 2009). Brains of staged larvae (96 hours after egg laying) were dissected in Schneider (Sigma) using sterile tools. Brains were transferred into tube containing 30 μ l of Schneider medium supplemented with 2,5% FBS and 1% streptomycin. 20 μ l of hemolymph was collected from larvae and carefully added to dissected brains. Co-cultures were incubated overnight at 18°C.

Immunofluorescence on larval tissues

Larval tissues were dissected in 1x PBS, fixed in 4% formaldehyde (Polyscience) in PBS for 30 min at room temperature and then washed several times in PBS containing 0,3% Triton X-100 (PBT). They were then blocked into PBT+10% FBS. Primary antibodies were incubated overnight at 4°C. After several washes, secondary antibodies were incubated 2h at room temperature. Dissected tissues were mounted into Vectashield (Vector). Fluorescence images were acquired using a Leica SP5 DS confocal microscope.

The following antibodies were used: rabbit anti Dsred (used to visualize mcherry) (1/200) (632496 Clontech), chicken anti GFP (1/10000) (ab13970 abcam), rat anti Dilp2 (1/400) (Géminard et al., 2009), rabbit anti Dilp5 (Géminard et al., 2009) rabbit anti pERK (1/200) (4370S Cell Signalling), rat anti HA (1/200) (3F10 Sigma). The rabbit anti ITK (Aedes locusta tachykinin used to visualize dTK) (1/500), rabbit anti CAPA precursor (1/500) (Kean et al., 2002), rabbit anti MIP (myoinhibitory peptide) (1/500) (Witek et al., 1999) and rabbit anti Dilp3 (1/1000) (Veenstra et al., 2008) were kindly gifted by J. Veenstra.

Fluorescence quantification

After acquisition of confocal z stacks of dissected tissue with a 0,5 μ m step and identical laser power and scan settings, images were analyzed by ImageJ. We performed the sum-intensity 3D projections to measure total fluorescent intensity across the object of interest (IPCs or ICNs) and subtracted the background fluorescent intensity. For a given experiment, all values are normalized to one control condition to give the “ Δ fluorescent intensity ratio” (Dilp2 or GFP accumulation). n represents the IPCs cluster or the ICNs number.

For ex-vivo organ culture presented in Fig 6E, GFP positive cells were counted instead of total fluorescent intensity. For a given experiment, all values are normalized to one control condition to give the “ Δ GFP positive cell ratio”. n represents the ICNs number.

Hemolymph collection

Hemolymph was collected as described in Rodenfels et al. (2014). It was obtained by bleeding larvae in ice cold PBS 1x. To remove hemocytes, a first centrifugation at 500g for 30min is performed and then followed by a second one at 16000g for 20min at 4°C to remove cellular fragments. The supernatant is then directly used for western blotting.

Protein extraction

After dissection, 5 to 10 fat bodies were transferred in an eppendorf with 60µl of RIPA buffer containing protease (Complete – Roche) and phosphatase inhibitor cocktails (Thermo Scientific). Tissues were then manually disrupted. Samples were then rotated for 30min at 4°C and then spun down at full speed, 4°C for 10min. Proteins were precipitated from the supernatant with chloroform-methanol mix (except for S2 cells extract). Pellets were dried 5 min and then dissolved into 1,5mM Tris, 6M Urea and inhibitor cocktails. Proteins measurements were done with the Bio-Rad Protein Assay (Bradford) (BIO-RAD).

Blue 4x (NuPage, Novex) and reducing agent 10x (NuPage, Novex) were added before heating at 100°C 5min.

Cell culture and phospho-MAPK assay

For the phospho-MAPK assay, on day 3 after transfection with *mt-egfr::V5*, S2R+ cells were treated with 100µM of CuSO₄ to induce EGFR::V5 expression. On day 4, cells transfected with *GAL4-UAS* plasmids were resuspended in Schneider medium and cocultured with EGFR::V5 expressing cells for 3 hours at 22°C. Cells were harvested and proteins were extracted.

Western Blotting

Proteins were resolved by SDS-PAGE 12% gels (NuPage, Novex gel, Invitrogen) using the MOPS running buffer and transferred electrophoretically to Nitrocellulose membranes (Biorad). Membranes were incubated 30 minutes in blocking buffer PBS-T (1X PBS, 0,1% Tween-20, 5% milk), and then incubated in the same buffer with primary antibodies, overnight at 4°C. After several washes, membranes were incubated 2h with PBS-T containing the secondary antibody and then washed again. Chemiluminescence was observed using the ECL Western Blotting detection system (ThermoFisher scientific). Images were taken with the Fujifilm Multi Gauge software and analyzed using imageJ.

The following antibodies were used: rabbit anti ERK (1/2000) (4695 Cell Signalling), rabbit anti pERK (1/2000) (4370S Cell Signalling), rat anti HA (1/500) (3F10 Sigma), guinea pig anti Cvd (1/2000) (gift from S. Eaton), mouse anti tubulin (1/2000) (T9026 Sigma).

Immunoprecipitation

A protein A or G-sepharose beads with CL6B beads mix was incubated with the primary antibody 3h at 4°C, after several washes in IP buffer (50mM Tris pH8, 150mM NaCl, 1mM EGTA, 10%NAF, protease (Complete – Roche) and phosphatase inhibitor cocktails (Thermo Scientific). After proteins extraction, 800µg of proteins were added to the mix and rotated at 4°C overnight. After several washes, blue 4x (NuPage, Novex) and reducing agent 10x (NuPage, Novex) were added and samples were heated at 100°C 5min.

The following antibodies were used: rabbit anti phospho-tyrosine (1/1000) (8654S Cell Signalling) and mouse anti V5 (1/2000) (R960-25 Invitrogen).

ELISA Test

Experimental procedure was adapted from Park et al. (2014). The ELISA plates were coated with anti-Flag (Sigma-Aldrich F1804) in coating buffer (0.2M sodium carbonate/bicarbonate buffer, pH9.4; [BuPH Carbonate-Bicarbonate buffer Packs ThermoFisher #28382](#)) and incubated overnight at 4°C. After several washes in PBS + 0,2% Tween 20 (PBTw0,2%), the plate was blocked in PBS + 2% BSA overnight at 4°C.

1µl or 2µl of hemolymph was transferred in 55µl of PBS, centrifuged at 1000g for 1min and 50µl of supernatant was transferred in PCR strips. As standards, the FLAG(GS)HA peptides (0-10ng/ml) are prepared in PCR strips. 5µl of diluted anti-HA-Peroxydase (High Affinity Roche 3F10, 12013819001) in PBTw0,2% (1/500) was added to samples/standards. After blockage, samples were transferred into the Nunc-Immuno modules and incubated overnight at 4°C. After several washes in PBTw0,2%, the Step Ultra TMB - ELISA Substrate (Thermo Scientific 34029) was added, incubated for 30 min at room temperature and then, 2M sulfuric acid was added to stop the reaction. Absorbance was measured at 450nm using the DLReady device (Berthold Technologies, Centro LB960).

n represents biological replicates.

Quantitative RT-PCR

qRT-PCR experimental procedure is described in (Delanoue et al., 2010). We dissected 15 brains per sample. n represents biological replicates.

Dilp2 primers: sense primer ATCTGGACGCCCTCAATCC and antisens primer
TCCCAGGAAAGAGGGCACTT

Dilp5 primers: sense primer GCCTGTCCCAATGGATTCAA and antisens primer
AGCTATCCAAATCCGCCAAGT

RP49 primers: sense primer CTTTCATCCGCCACCAGTC and antisens primer CGACGCACTCTGTTGTTCG

Wing analysis

Adult flies were collected, stored in ethanol and wings were mounted in Euparal solution. Pictures were acquired using a Leica Fluoresce StereomicroScope M205 FA with a Leica digital camera MC 190 HD. n represents the wings number.

Quantification and Statistical Analysis

P values are the result of ANOVA or Student's t test provided by Graphpad Prism (* $p < 0,05$; ** $p < 0,01$; *** $p < 0,001$, **** $p < 0,0001$). Significance of calcium activity quantification in Figure 3 and Figure 6D and 6E were calculated with Student's t test. Statistical analyses of the other figures were performed using one-way ANOVA.

Supplemental information titles and legends

Figure S1: Complete expression pattern of the R22H11 driver. Related to Figure 1

A. The *R22H11-GAL4* line drives mCD8GFP (green) in one neuron in each brain hemisphere, (hereafter referred as ICNs, see text) indicated by an asterisk*, and in one pair of CAPA positive neurons (red), shown with a white arrowhead. CC: Corpora Cardiaca SEG: Subesophageal ganglion

Figure S2: Overgrowth phenotypes are exclusively due to the ICNs effect on Dilps secretion, with no effect on developmental timing, feeding behavior nor dilp2 expression. Related to Figure 2.

A. Pupal volume measurements in all control conditions (*icn>w, w UAS-*). (n>94)

B. Pupal volume measurements after CAPA neurons ablation (*capa>hid*), hyperpolarization (*capa>kir2.1*), blockade of secretory activity (*capa>tetx*) or chronic depolarization (*capa>nachbac*). (n>60)

C. Developmental timing measurements after ICNs ablation (*icn>hid*). (n>40)

D. Feeding behavior was tested after ICNs ablation (*icn>hid*). (n=9)

E. *dilp2* mRNA levels in dissected brains were quantified upon ICNs ablation (*icn>hid*), hyperpolarization (*icn>kir2.1*), secretion blockade (*icn>tetx*) or depolarization (*icn>nachbac*). (n=3)

F. *dilp5* mRNA levels in dissected brains were quantified upon ICNs ablation (*icn>hid*), hyperpolarization (*icn>kir2.1*), secretion blockade (*icn>tetx*) or depolarization (*icn>nachbac*). (n=3)

G. Dilp5 accumulation levels in the IPCs upon ICNs ablation (*icn>hid*), hyperpolarization (*icn>kir2.1*) secretion blockade (*icn>tetx*) or depolarization (*icn>nachbac*). (n>40) Fluorescence intensity is measured as delta ratio compared to control (*icn>w*).

H. Dilp3 accumulation levels in the IPCs upon ICNs ablation (*icn>hid*), hyperpolarization (*icn>kir2.1*) secretion blockade (*icn>tetx*) or depolarization (*icn>nachbac*). (n>40) Fluorescence intensity is measured as delta ratio compared to control (*icn>w*).

In graphs, means are shown and errors bars represent \pm SEM.

Figure S3: GBPs stimulate body growth specifically through ICNs. Related to Figure 4.

A. Pupal volume measurements in all control conditions (*icn>w*, *w UAS-*). (n>60)

B. Pupal volume measurements upon ectopic expressions of the fat body signals *sun* (*icn>sun*) and *upd2* (*icn>upd2*) in ICNs. (n>144)

C. Pupal volume measurements upon *gbp1* (*lpp>gbp1*) or *gbp2* (*lpp>gbp2*) overexpression in the fat body. (n>67)

D. Pupal volume measurements upon ectopic expressions of *gbp1* and *gbp2* in the EH (eclosion hormone) neurons (*eh>gbp1* and *eh>gbp2*). (n>75)

E. Pupal volume measurements upon ectopic expressions of *gbp1* and *gbp2* in the CAPA neurons (*capa>gbp1* and *capa>gbp2*). (n>88)

F. *gbp1* overexpression in the fat body using *lpp-GAL4* driver (*lpp>gbp1*) does not induce extra veins (L2). (n>15)

In graphs, means are shown and errors bars represent \pm SEM, ****p<0,0001, **p<0,01.

Figure S4: Activation of EGFR signaling in ICNs promotes body growth via its effect on Dilps secretion without altering the ICNs identity nor dilps expression. Related to Figure 5.

A. Pupal volume measurements in all control conditions (*icn>w*, *w UAS-*). (n>44)

B. Quantification of *dilp2* mRNA levels in dissected brains upon EGFR signaling pathway inhibition (*icn>egfrRi* and *icn>dsorRi*) or activation (*icn>egfr^{A887T}*) in the ICNs. (n=3)

C. Pupal volume measurements upon EGFR signaling pathway inhibition (*capa>egfrRi*, *capa>dsorRi*) or activation (*capa>egfr^{A887T}*) in the CAPA neurons. (n>83)

D. Pupal volume measurements upon ectopic expressions in the ICNs of a secreted activated form of Spitz (*icn>sspi*), its membrane-tethered form (*icn>UAS-nrt::sspi*) or the unprocessed form of Spitz (*icn>UASmspi*). (n>62)

E-E'. ICNs labelled by GFP (green) and either dTK (tachykinin) (E, red) or MIP (Myoinhibitory peptide) (E', red) antibodies upon EGFR signaling inhibition (*icn>mCD8GFP*, *egfrRi* and *-dsorRi*) or activation (*icn>mCD8GFP*, *egfr^{A887T}*).

F. Pupal volumes after ectopic expression of *gbp1* alone (*icn>gbp1*), or upon co-silencing *dsor* (*icn>dsorRi,gbp1*) in the ICNs. (n>55)

In graphs, means are shown and errors bars represent \pm SEM, ****p<0,0001, **p<0,01, *p<0,05.

Figure S5: The fusion protein GBP1::HA is functional and can be used to study secretion and localization of GBP1. Related to Figure 6.

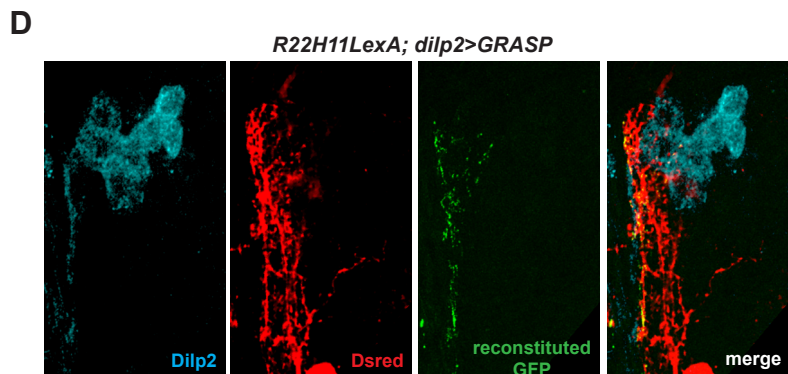
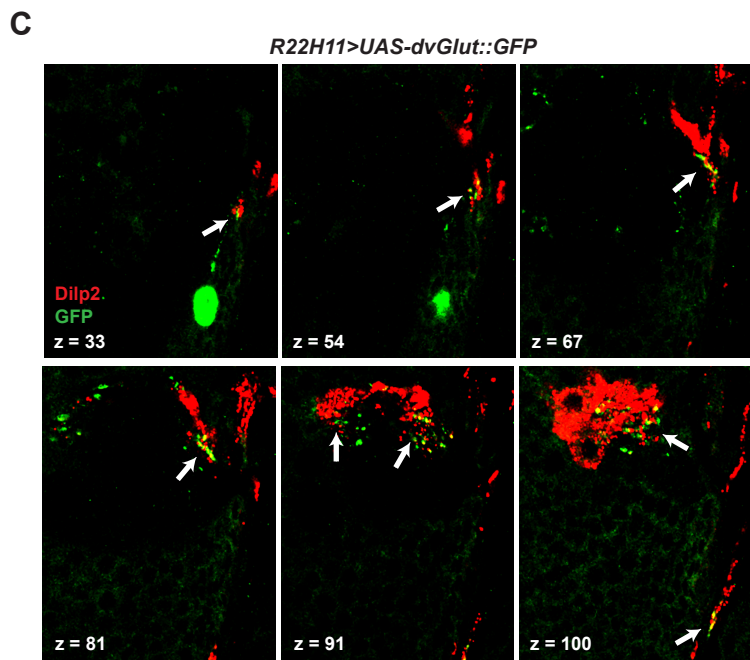
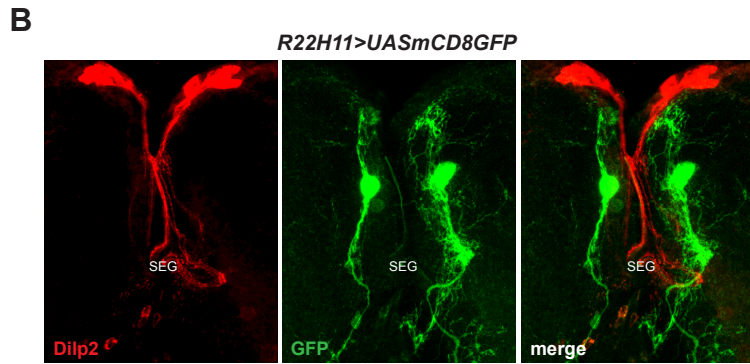
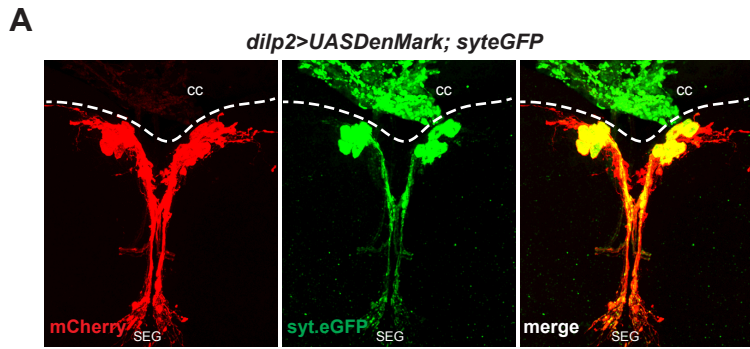
A. Pupal volumes after overexpression of the fusion protein GBP1::HA in the fat body (*lpp>gbp1::HA*). (n>48)

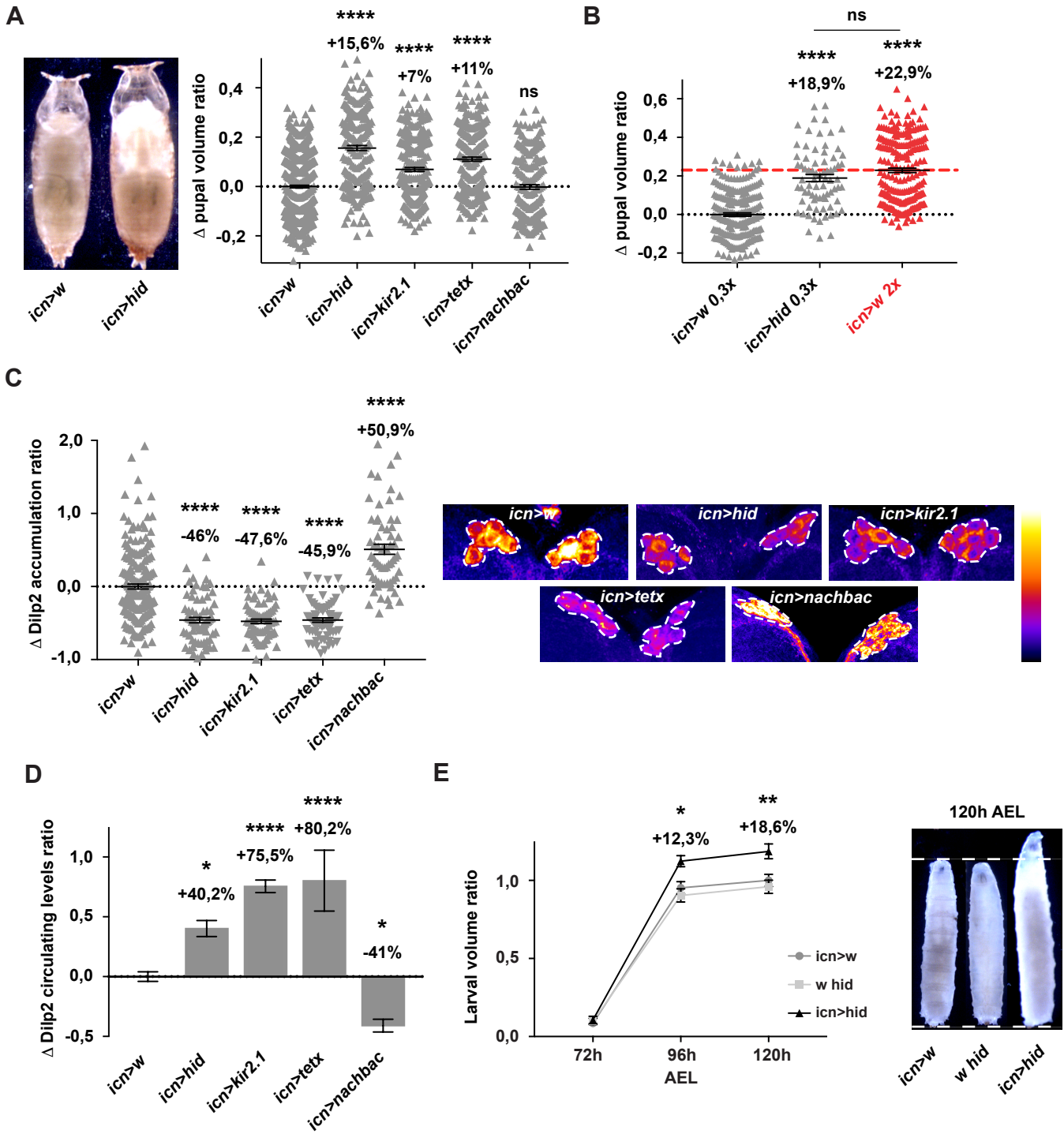
B. Pupal volumes after overexpression of the fusion protein GBP1::HA in the ICNs (*icn>gbp1::HA*). (n>62)

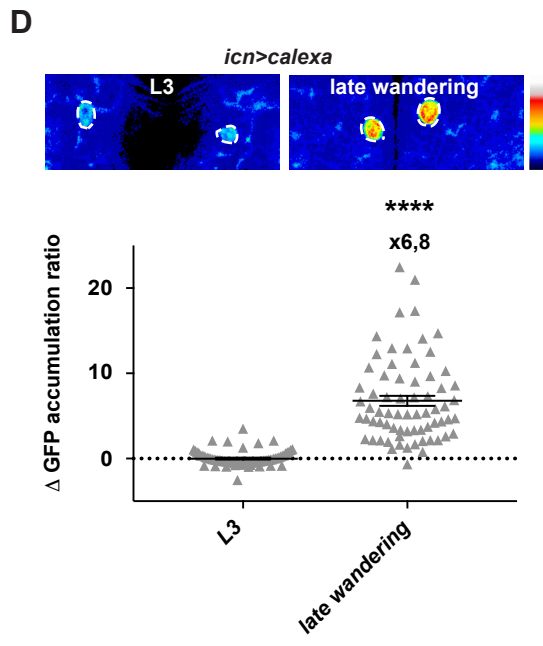
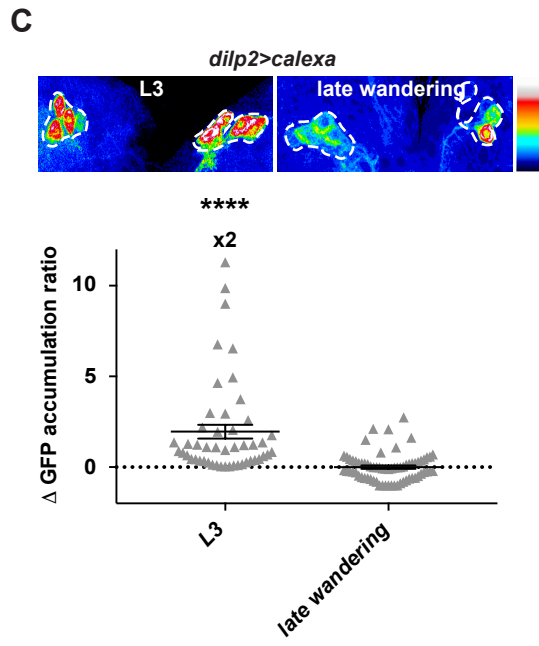
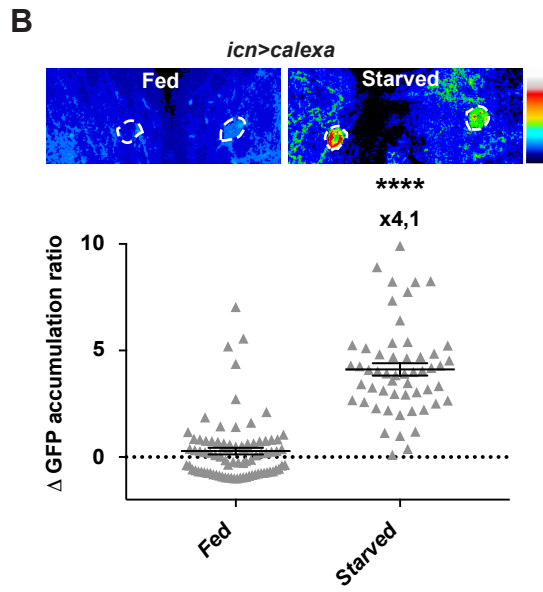
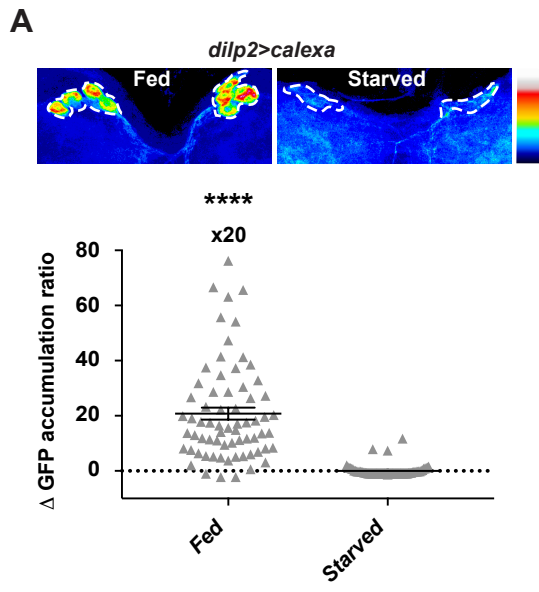
C. GBP1::HA containing vesicles stained in the fat body upon fed condition and acute amino acids starvation (*lpp>gbp1::HA*). Scale bar represents 2,5 μ m.

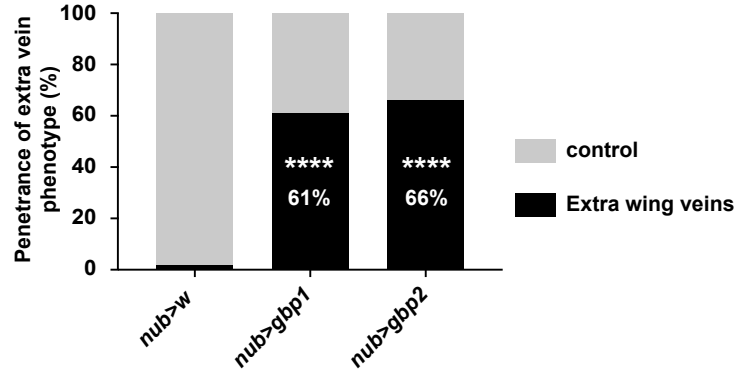
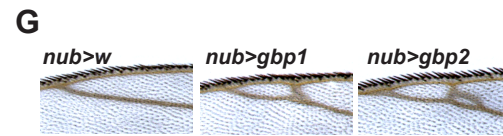
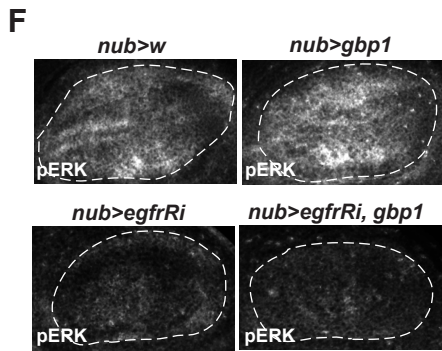
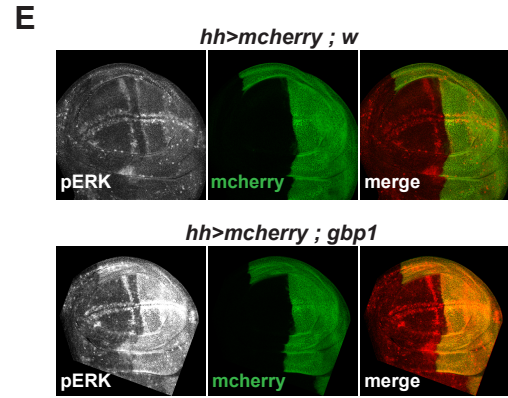
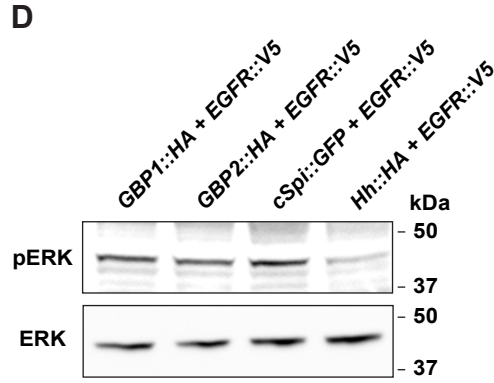
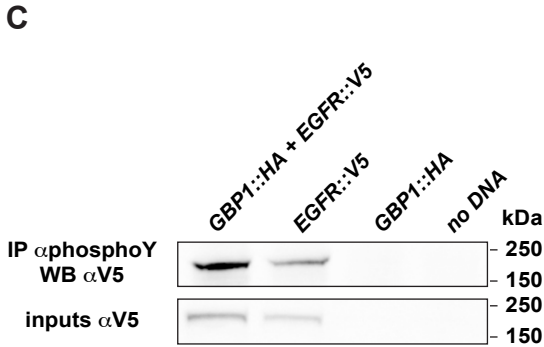
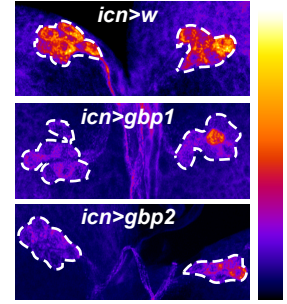
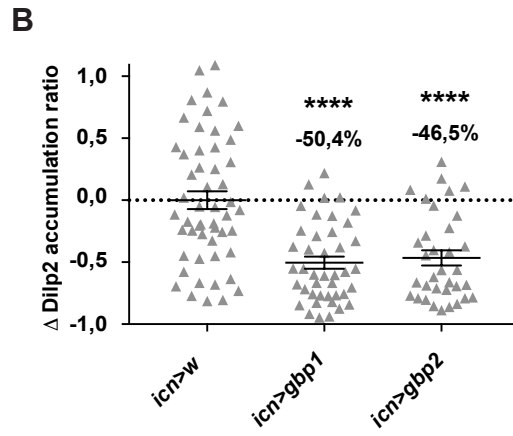
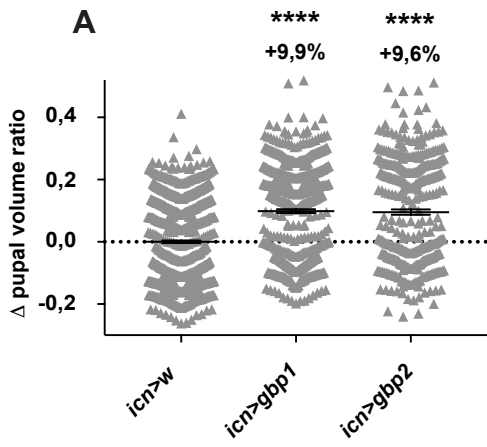
D. GBP1::HA (green) stainings in the ICNs, labelled with dTK (red) antibody in control genotypes (*lpp>w* and *w gbp1::HA*).

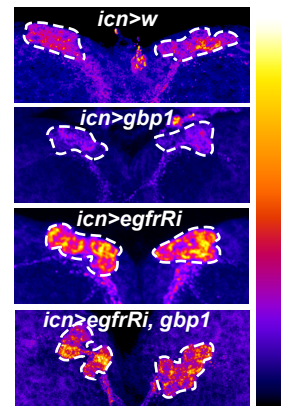
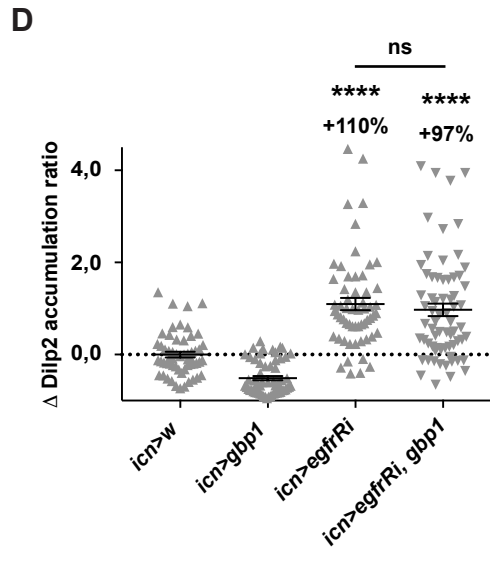
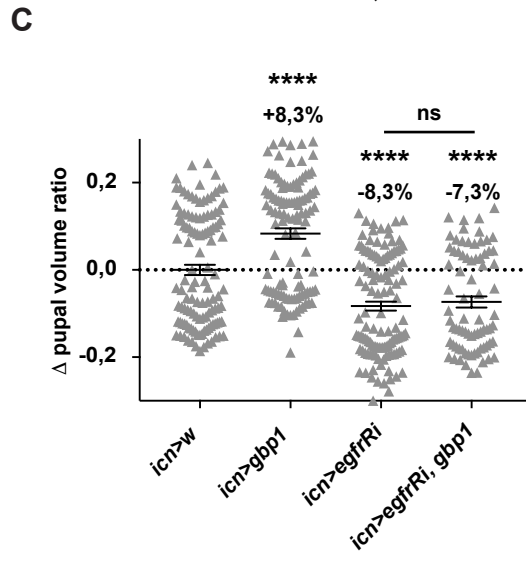
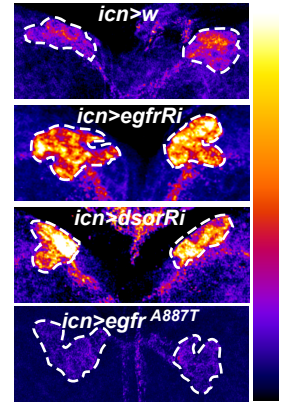
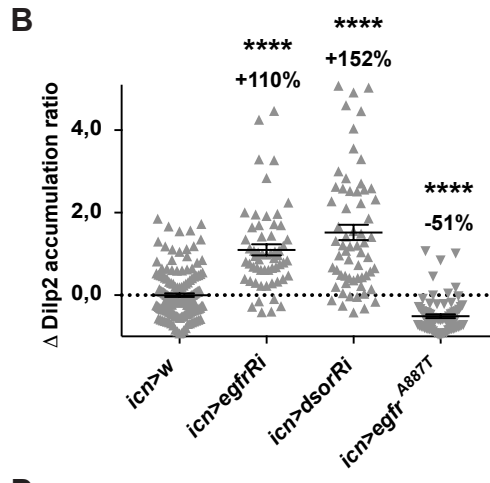
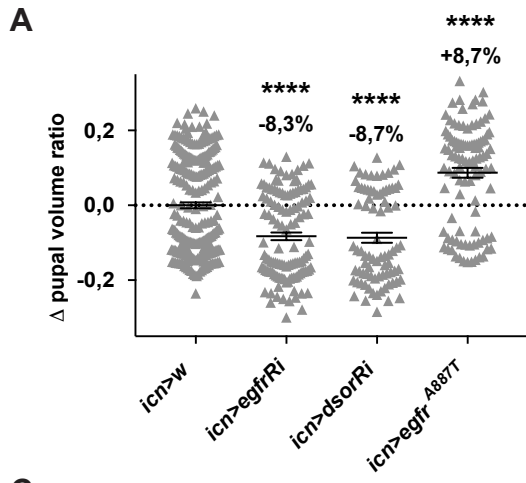
In graphs, means are shown and errors bars represent \pm SEM, ****p<0,0001, **p<0,01, *p<0,05.

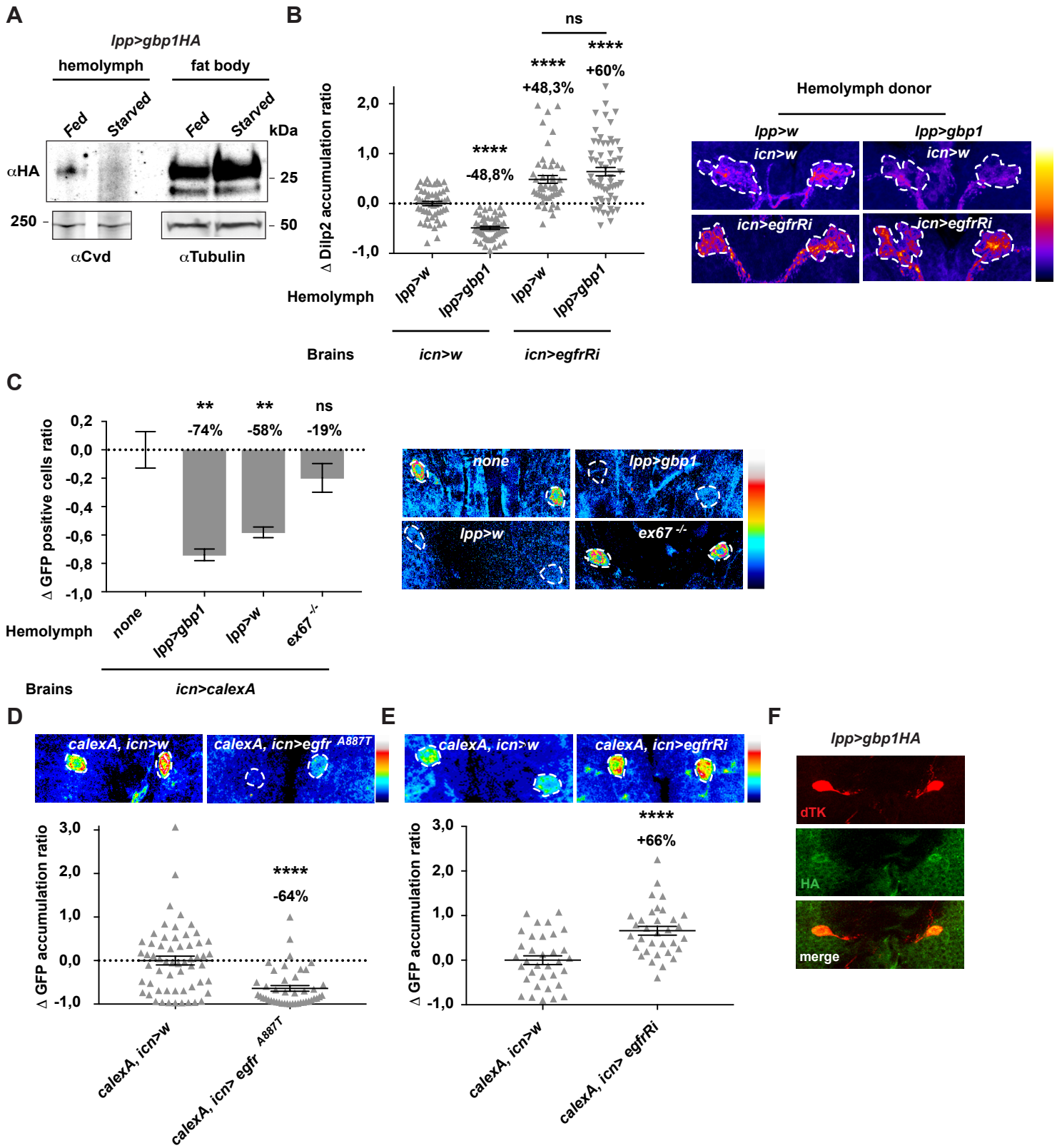












KEY RESOURCES TABLE

REAGENT or RESOURCE	SOURCE	IDENTIFIER
Antibodies		
Rabbit polyclonal anti Dsred	Clontech	Cat#632496, RRID:AB_10013483
Chicken polyclonal anti GFP	Abcam	mAb13970, RRID:AB_300798
Rat polyclonal anti Dilp2	(Géminard et al., 2009)	N/A
Rabbit polyclonal anti Dilp5	(Géminard et al., 2009)	N/A
Rabbit monoclonal anti pERK	Cell signaling Technology	Cat#4370S, RRID:AB_2315112
Rabbit monoclonal anti ERK	Cell signaling Technology	Cat#4695, RRID:AB_390779
Rat monoclonal anti HA	Sigma Aldrich	Cat#3F10, RRID:AB_10094468
Rabbit polyclonal anti <i>Aedes locusta</i> Tachykinin	(Veenstra et al., 2008)	N/A
Rabbit polyclonal anti CAPA-precursor	(Kean et al., 2002)	N/A
Rabbit polyclonal anti MIP	(Witek et al., 1999)	N/A
Rabbit polyclonal anti Ilp3	(Veenstra et al., 2008)	N/A
Guinea pig polyclonal anti Cvd	(Brankatschk et al., 2014)	N/A
Mouse monoclonal anti Tubulin	Sigma Aldrich	Cat#T9026, RRID:AB_477593
Mouse monoclonal anti V5	ThermoFisher Scientific - Invitrogen	Cat#R960-25, RRID:AB_2556564
Rabbit monoclonal anti phosphor-tyrosine	Cell signaling Technology	Cat#8954S, RRID:AB_2687925
Mouse monoclonal anti FLAG	Sigma Aldrich	Cat#F1804 RRID:AB_262044
Chemicals, Peptides, and Recombinant Proteins		
Erioglaucine disodium salt	Sigma Aldrich	Cat#861146
Schneider's Insect Medium	Sigma Aldrich	Cat#S0146
Lipofectamine	ThermoFisher Scientific	Cat#18324012
Formaldehyde	Polysciences, Inc.	Cat#18814-10
Vectashield	VECTOR Laboratories	Cat#H-1200
cOmplete Protease inhibitor cocktail	Sigma Aldrich Roche	Cat#11697498001
Halt™ Phosphatase Inhibitor Cocktail	ThermoFisher Scientific	Cat#78420
Bio-Rad Protein Assay	BIORAD	Cat#500-0006
Pierce™ ECL Western Blotting Substrate	ThermoFisher Scientific	Cat#32106
Euparal	Roth	Cat#7356.1
BupH™ Carbonate-Bicarbonate Buffer Packs	ThermoFisher Scientific	Cat#28382
Step™ Ultra TMB-ELISA Substrate Solution	ThermoFisher Scientific	Cat#34029
Critical Commercial Assays		
pENTR™/D-TOPO Cloning Kit	ThermoFisher Scientific - Invitrogen	Cat#K2400-20
Experimental Models: Cell Lines		
S2R+ cells	Drosophila Genomics Resource Center	Cat#150, RRID:CVCL_Z831
Experimental Models: Organisms/Strains		

<i>Drosophila</i> : w ¹¹¹⁸	Bloomington <i>Drosophila</i> Stock Center	RRID:BDSC_3605
<i>Drosophila</i> : Dilp2-GAL4	(Rulifson et al., 2002)- Bloomington <i>Drosophila</i> Stock Center	RRID:BDSC_37516
<i>Drosophila</i> : Hh-GAL4	(Tanimoto et al., 2000)	N/A
<i>Drosophila</i> : Lpp-GAL4	(Brankatschk and Eaton, 2010)	N/A
<i>Drosophila</i> : Lsp2-GAL4	Bloomington <i>Drosophila</i> Stock Center	RRID:BDSC_6357
<i>Drosophila</i> : lexAop-CD8-GFP-2A-CD8-GFP; UAS-mLexA-VP16-NFAT, LexAop-rCD2-GFP	(Masuyama et al., 2012) - Bloomington <i>Drosophila</i> Stock Center	RRID:BDSC_66542
<i>Drosophila</i> : UAS-dvglut::GFP	(Riemensperger et al., 2013)	N/A
<i>Drosophila</i> : UAS-sun	(Delanoue et al., 2016)	N/A
<i>Drosophila</i> : UAS-upd2	(Hombria et al., 2005)	N/A
<i>Drosophila</i> : UAS-gbp1	(Koyama and Mirth, 2016)	N/A
<i>Drosophila</i> : UAS-gbp2	(Koyama and Mirth, 2016)	N/A
<i>Drosophila</i> : ex67 ^{-/-}	(Koyama and Mirth, 2016)	N/A
<i>Drosophila</i> : UAS-mspi	(Schweitzer et al., 1995)	N/A
<i>Drosophila</i> : UAS-sspi	(Schweitzer et al., 1995)	N/A
<i>Drosophila</i> : UAS-nrt::sspi	(Steinhauer et al., 2013)	N/A
<i>Drosophila</i> : R22H11-GAL4	(Pfeiffer et al., 2010) - Bloomington <i>Drosophila</i> Stock Center	RRID:BDSC_48043
<i>Drosophila</i> : R22H11LexA	Bloomington <i>Drosophila</i> Stock Center	RRID:BDSC_54109
<i>Drosophila</i> : UAS-egfr RNAi 107130KK	Vienna <i>Drosophila</i> Resource Center	RRID:VDRC_107130
<i>Drosophila</i> : UAS-dsor RNAi 107276KK	Vienna <i>Drosophila</i> Resource Center	RRID:VDRC_107276
<i>Drosophila</i> : nubbin-GAL4	(Azpiazu and Morata, 2000)	N/A
<i>Drosophila</i> : UAS-hid	Bloomington <i>Drosophila</i> Stock Center	RRID:BDSC_65403
<i>Drosophila</i> : UAS-tetx	Bloomington <i>Drosophila</i> Stock Center	RRID:BDSC_28838
<i>Drosophila</i> : UAS-kir2.1	Bloomington <i>Drosophila</i> Stock Center	RRID:BDSC_6595
<i>Drosophila</i> : UAS-NaChBac	Bloomington <i>Drosophila</i> Stock Center	RRID:BDSC_9469
<i>Drosophila</i> : UAS-egfr ^{A88T}	Bloomington <i>Drosophila</i> Stock Center	RRID:BDSC_9333
<i>Drosophila</i> : Eh-GAL4	Bloomington <i>Drosophila</i> Stock Center – (McNabb et al., 1997)	RRID:BDSC_6301
<i>Drosophila</i> : UAS-mCD8GFP	Bloomington <i>Drosophila</i> Stock Center	RRID:BDSC_32185

<i>Drosophila</i> : UAS-mCherry	Bloomington <i>Drosophila</i> Stock Center	RRID:BDSC_27392
<i>Drosophila</i> : Capa-GAL4	Bloomington <i>Drosophila</i> Stock Center	RRID:BDSC_45895
<i>Drosophila</i> : UAS-DenMark, UAS-syteGFP	Bloomington <i>Drosophila</i> Stock Center	RRID:BDSC_33065
<i>Drosophila</i> : LexAop-rCD2-RFP ; UAS-CD4-spGFP1-10, LexAop-CD4-spGFP11	Bloomington <i>Drosophila</i> Stock Center	RRID:BDSC_58755
<i>Drosophila</i> : UAS-gbp1 ::HA	This study	N/A
<i>Drosophila</i> : gd2HF (Chr.2)	This study	N/A
Oligonucleotides		
Primer: GBP1 Forward: CACCGAATTCAGGATGTTGATACGTATTAATCCA TTGGTG Reverse: CCGGAATTCCGCCGGCTTTCTGCATCGTTTTCC	This study	N/A
Primer: GBP2 Forward: CACCGGTACCAGGATGTTTTTGCAACTCTTATCT ATA Reverse: CCGGGTACCGGCTTCCTTCCTGCAACGTCCTGC	This study	N/A
Primer: Dilp2 Forward: ATCTGGACGCCCTCAATCC Reverse: TCCCAGGAAAGAGGGCACTT	(Slaidina et al., 2009)	N/A
Primer: Dilp5 Forward: GCCTGTCCCAATGGATTCAA Reverse: AGCTATCCAAATCCGCCAAGT	(Slaidina et al., 2009)	N/A
Primer: RP49 Forward: CTTTCATCCGCCACCAGTC Reverse: CGACGCACTCTGTTGTCCG	(Slaidina et al., 2009)	N/A
Recombinant DNA		
pTWH	<i>Drosophila</i> Genomics Resource Center	Cat#1100
pBDP2 gdilp2-BHA-FLAGA	(Park et al., 2014)	N/A
mt-egfr::V5	(Schweitzer et al., 1995)	N/A
UAS-cSpi::GFP	(Tsruya et al., 2002)	N/A
UAS-Hh::HA	(Burke et al., 1999)	N/A
UAS-gbp1::HA	This study	N/A
UAS-gbp2::HA	This study	N/A
cDNA clone GBP1 IP05665	<i>Drosophila</i> Genomics Resource Center	Cat#1382281 Flybase: FBgn0034199
cDNA clone GBP2 GH14572	<i>Drosophila</i> Genomics Resource Center	Cat#7552 Flybase: FBgn0034200

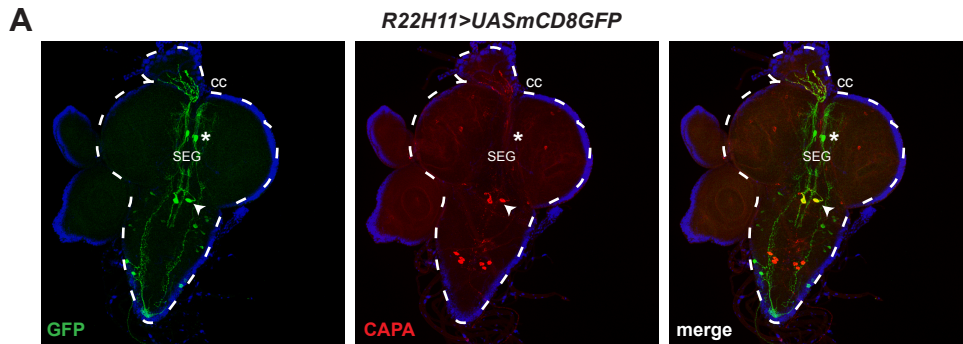


Figure S1: Complete expression pattern of the R22H11 driver. Related to Figure 1
A. The *R22H11-GAL4* line drives mCD8GFP (green) in one neuron in each brain hemisphere, (hereafter referred as ICNs, see text) indicated by an asterisk*, and in one pair of CAPA positive neurons (red), shown with a white arrowhead. CC: Corpora Cardiacia SEG: Subesophageal ganglion

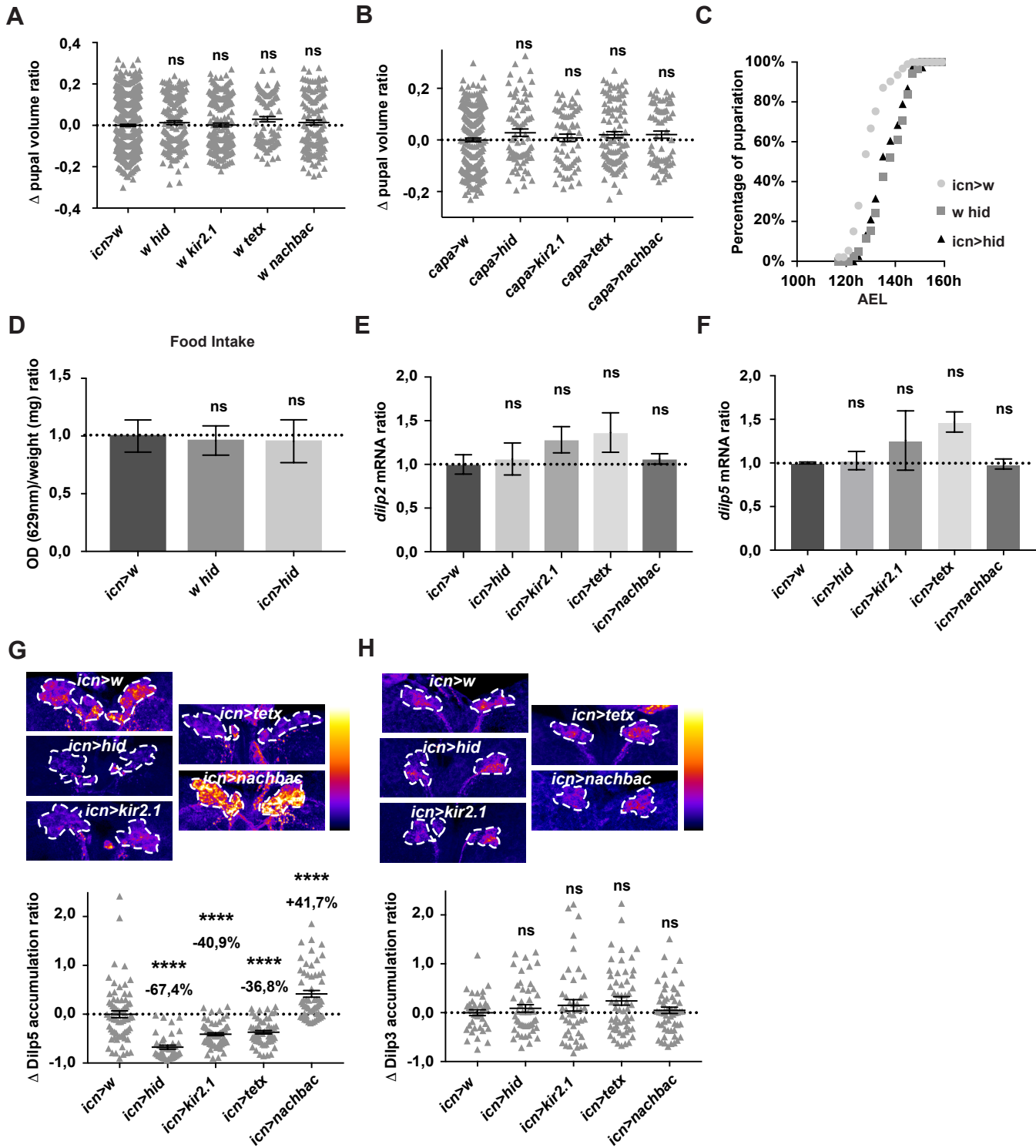


Figure S2: Overgrowth phenotypes are exclusively due to the ICNs effect on Dilps secretion, with no effect on developmental timing, feeding behavior nor dilp2 expression. Related to Figure 2.

A. Pupal volume measurements in all control conditions (*icn>w*, *w UAS-*). (n>94)

B. Pupal volume measurements after CAPA neurons ablation (*capa>hid*), hyperpolarization (*capa>kir2.1*), blockade of secretory activity (*capa>tetx*) or chronic depolarization (*capa>nachbac*). (n>60)

C. Developmental timing measurements after ICNs ablation (*icn>hid*). (n>40)

D. Feeding behavior was tested after ICNs ablation (*icn>hid*). (n=9)

E. *dilp2* mRNA levels in dissected brains were quantified upon ICNs ablation (*icn>hid*), hyperpolarization (*icn>kir2.1*), secretion blockade (*icn>tetx*) or depolarization (*icn>nachbac*). (n=3)

F. *dilp5* mRNA levels in dissected brains were quantified upon ICNs ablation (*icn>hid*), hyperpolarization (*icn>kir2.1*), secretion blockade (*icn>tetx*) or depolarization (*icn>nachbac*). (n=3)

G. Dilp5 accumulation levels in the IPCs upon ICNs ablation (*icn>hid*), hyperpolarization (*icn>kir2.1*) secretion blockade (*icn>tetx*) or depolarization (*icn>nachbac*). (n>40) Fluorescence intensity is measured as delta ratio compared to control (*icn>w*).

H. Dilp3 accumulation levels in the IPCs upon ICNs ablation (*icn>hid*), hyperpolarization (*icn>kir2.1*) secretion blockade (*icn>tetx*) or depolarization (*icn>nachbac*). (n>40) Fluorescence intensity is measured as delta ratio compared to control (*icn>w*).

In graphs, means are shown and errors bars represent \pm SEM.

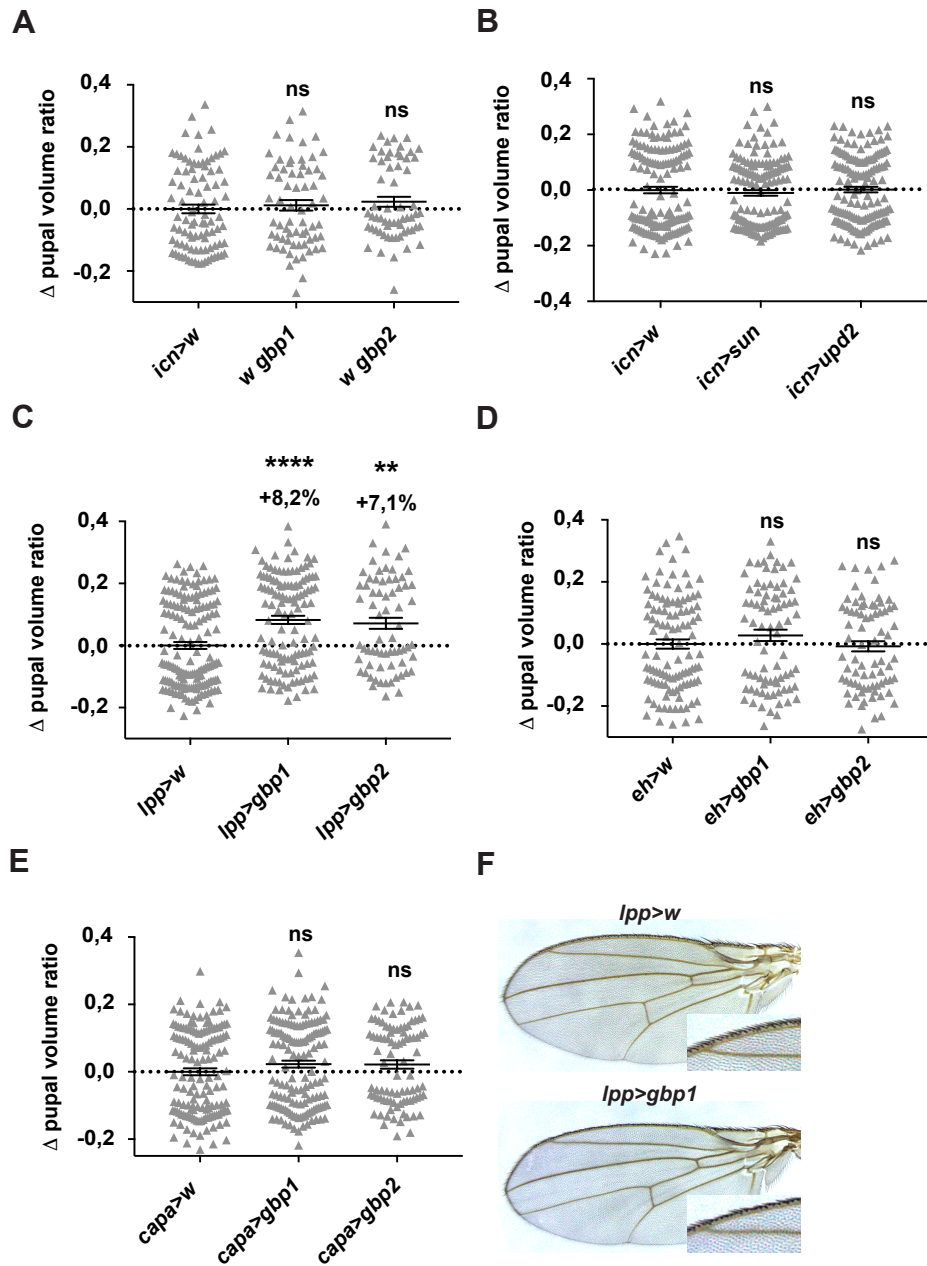


Figure S3: GBPs stimulate body growth specifically through ICNs. Related to Figure 4.

A. Pupal volume measurements in all control conditions (*icn>w*, *w UAS*-). (n>60)

B. Pupal volume measurements upon ectopic expressions of the fat body signals *sun* (*icn>sun*) and *upd2* (*icn>upd2*) in ICNs. (n>144)

C. Pupal volume measurements upon *gbp1* (*lpp>gbp1*) or *gbp2* (*lpp>gbp2*) overexpression in the fat body. (n>67)

D. Pupal volume measurements upon ectopic expressions of *gbp1* and *gbp2* in the EH (eclosion hormone) neurons (*eh>gbp1* and *eh>gbp2*). (n>75)

E. Pupal volume measurements upon ectopic expressions of *gbp1* and *gbp2* in the CAPA neurons (*capa>gbp1* and *capa>gbp2*). (n>88)

F. *gbp1* overexpression in the fat body using *lpp-GAL4* driver (*lpp>gbp1*) does not induce extra veins (L2). (n>15)

In graphs, means are shown and errors bars represent \pm SEM, ****p<0,0001, **p<0,01.

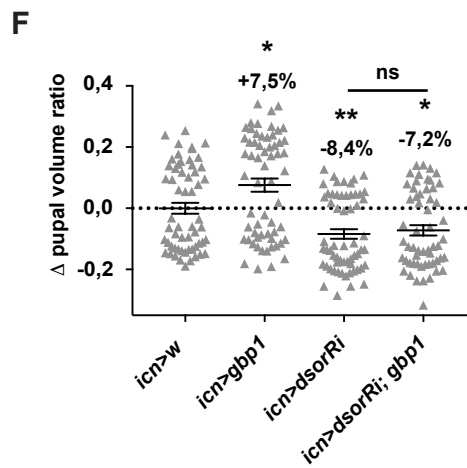
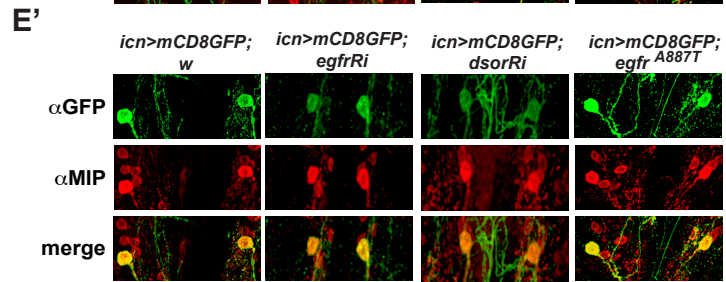
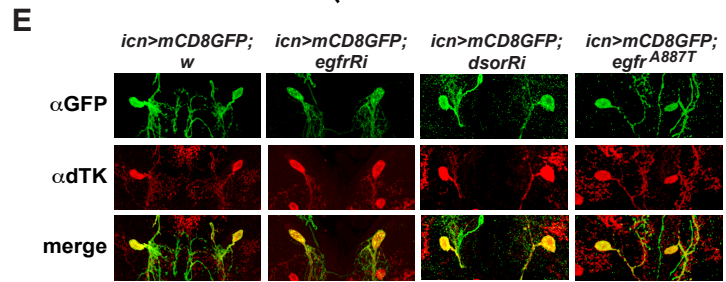
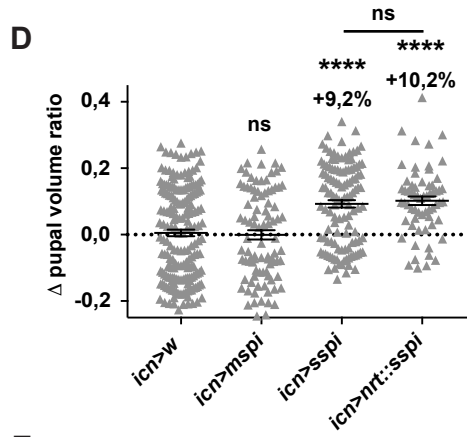
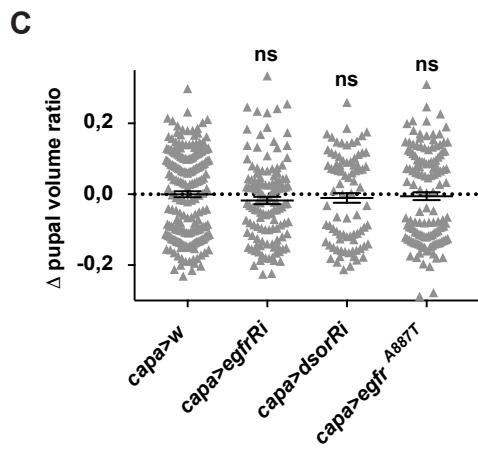
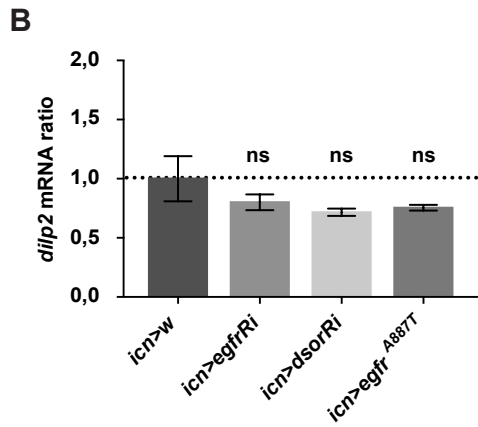
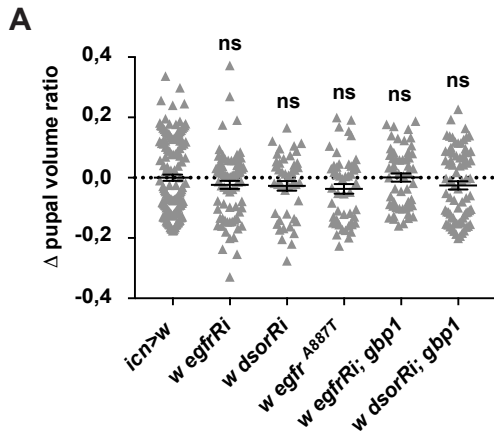


Figure S4: Activation of EGFR signaling in ICNs promotes body growth via its effect on Dilps secretion without altering the ICNs identity nor dilps expression. Related to Figure 5.

A. Pupal volume measurements in all control conditions (*icn>w, w UAS-*). (n>44)

B. Quantification of *dilp2* mRNA levels in dissected brains upon EGFR signaling pathway inhibition (*icn>egfr^{Ri}* and *icn>dsor^{Ri}*) or activation (*icn>egfr^{A887T}*) in the ICNs. (n=3)

C. Pupal volume measurements upon EGFR signaling pathway inhibition (*capa>egfr^{Ri}*, *capa>dsor^{Ri}*) or activation (*capa>egfr^{A887T}*) in the CAPA neurons. (n>83)

D. Pupal volume measurements upon ectopic expressions in the ICNs of a secreted activated form of Spitz (*icn>sspi*), its membrane-tethered form (*icn>UAS-nrt::sspi*) or the unprocessed form of Spitz (*icn>UASmspi*). (n>62)

E-E'. ICNs labelled by GFP (green) and either dTK (tachykinine) (E, red) or MIP (Myoinhibitory peptide) (E', red) antibodies upon EGFR signaling inhibition (*icn>mCD8GFP, egfr^{Ri}* and *-dsor^{Ri}*) or activation (*icn>mCD8GFP, egfr^{A887T}*).

F. Pupal volumes after ectopic expression of *gbp1* alone (*icn>gbp1*), or upon co-silencing *dsor* (*icn>dsor^{Ri}, gbp1*) in the ICNs. (n>55)

In graphs, means are shown and errors bars represent \pm SEM, ****p<0,0001, **p<0,01, *p<0,05.

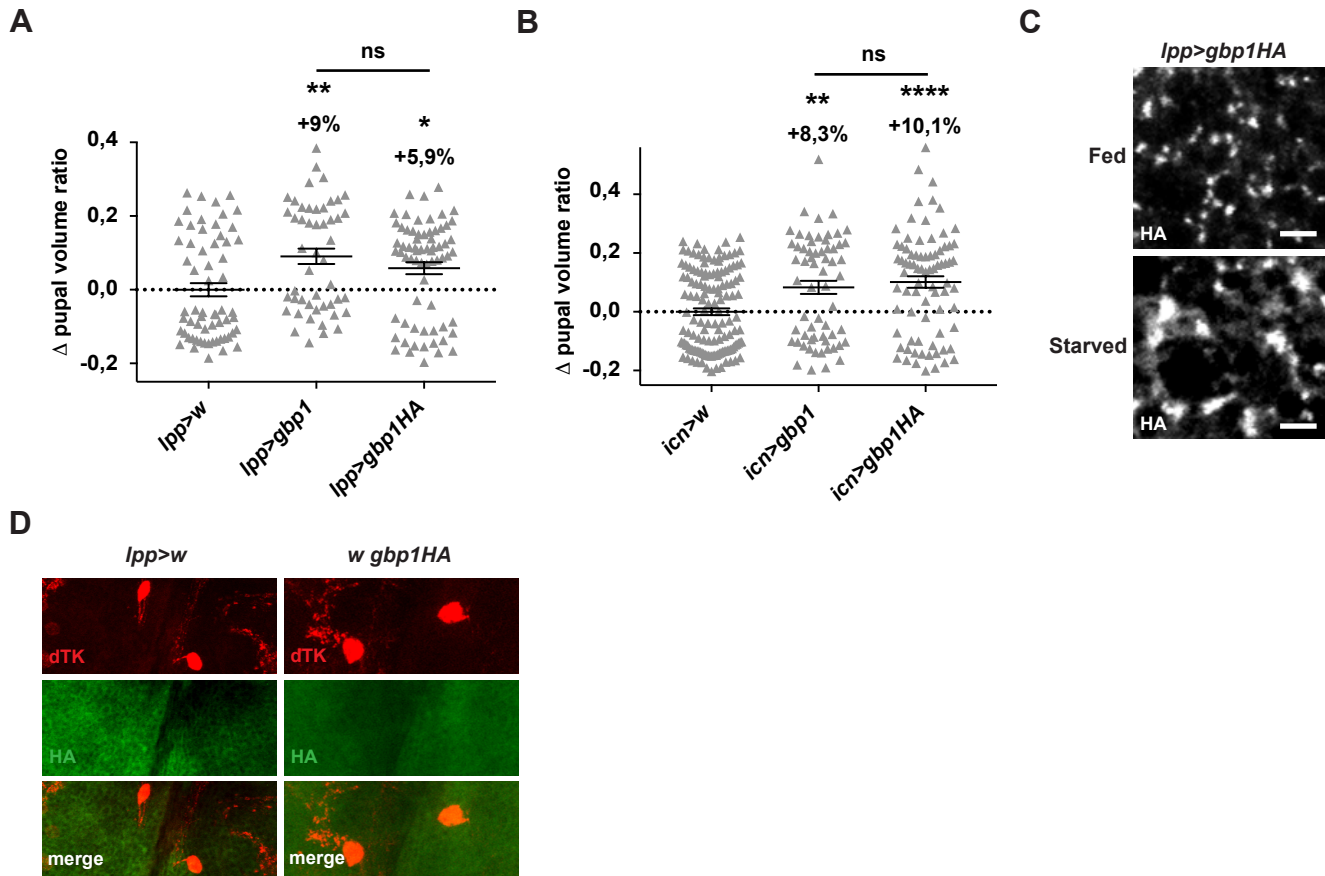


Figure S5: The fusion protein GBP1::HA is functional and can be used to study secretion and localization of GBP1. Related to Figure 6.

A. Pupal volumes after overexpression of the fusion protein GBP1::HA in the fat body (*lpp>gbp1::HA*). (n>48)

B. Pupal volumes after overexpression of the fusion protein GBP1::HA in the ICNs (*icn>gbp1::HA*). (n>62)

C. GBP1::HA containing vesicles stained in the fat body upon fed condition and acute amino acids starvation (*lpp> gbp1::HA*). Scale bar represents 2,5 μ m.

D. GBP1::HA (green) stainings in the ICNs, labelled with dTK (red) antibody in control genotypes (*lpp>w* and *w gbp1::HA*).

In graphs, means are shown and errors bars represent \pm SEM, ****p<0,0001, **p<0,01, *p<0,05.